





Jomo Kenyatta University of Agriculture and Technology  
College of Engineering and Technology  
School of Mechanical, Materials, and Manufacturing Engineering  
Department of Mechatronic Engineering

---

# **Design and Fabrication of a Dual Recovery System for the N4 Rocket**

**FYP-20-1**

**(Final Year Project Report)**

Ian Kiptoo (ENM221-0067/2019)

Kennedy Mwendwa (ENM221-0199/2019)

**SUPERVISOR**

Dr. Shohei Aoki

**TECHNOLOGIST**

Mr. Joseph Matunda

January 2025

---

## Declaration

We hereby declare that the work contained in this report is original; researched and documented by the undersigned students. It has not been used or presented elsewhere in any form for award of any academic qualification or otherwise. Any material obtained from other parties have been duly acknowledged. We have ensured that no violation of copyright or intellectual property rights have been committed.

1. Ian Kiptoo

Signature..... Date.....

2. Kennedy Mwendwa

Signature..... Date.....

Approved by supervisors:

1. Dr. Shohei Aoki

Signature..... Date.....

## Abstract

In high-power rocketry, recovery systems are vital for ensuring safe descent and reuse. Single-parachute systems often lead to excessive drift and recovery challenges, particularly in high-altitude flights. This project focuses on the design, development, and implementation of a dual recovery system for the N4 high-power rocket to address these limitations. The system employs two parachutes deployed at different stages of descent: a drogue parachute at apogee stabilizes the initial descent without significant drift, and a main parachute at a lower altitude ensures controlled and safe landing near the launch site. The avionics bay, doubling as a structural coupler, houses the flight computer that manages the ejection charges to enable precise deployment.

The methodology involved selecting descent velocities that adhere to Spaceport America Cup requirements—20-50 m/s for drogue descent and below 10 m/s for main descent. Based on the N4 rocket's 26 kg weight, target velocities were set to 21 m/s for drogue descent and 5.5 m/s for main descent. Parachute diameters were calculated to achieve these terminal velocities. Altitude, velocity, acceleration, and orientation data were refined using a Kalman filter, integrating measurements from a barometric pressure sensor and an MPU6050 accelerometer. A state machine was developed to manage flight stages, from preflight to postflight, ensuring precise deployment timing.

The avionics bay was fabricated to house the flight computer and connect rocket sections securely. Parachutes were enclosed with shear pins to prevent premature ejection, while ejection charges using crimson powder ensured reliable deployment. The system was rigorously tested and successfully achieved its design objectives, demonstrating safe descent and controlled landing in real-world conditions.

# Contents

<b>Declaration</b> . . . . .	<b>I</b>
<b>Abstract</b> . . . . .	<b>II</b>
<b>1 Introduction</b> . . . . .	<b>1</b>
1.1 Problem Statement: . . . . .	2
1.2 Objectives . . . . .	3
1.2.1 Main Objective: . . . . .	3
1.2.2 Specific Objectives: . . . . .	3
1.3 Scope . . . . .	3
1.4 Justification: . . . . .	4
<b>2 Literature Review</b> . . . . .	<b>5</b>
2.1 History of Dual Recovery Systems . . . . .	5
2.2 Operation Sequence . . . . .	6
2.3 Comparison of Parachute Types . . . . .	9
2.3.1 Parachute Design and Sizing . . . . .	10
2.3.2 Materials Used in Parachute Fabrication . . . . .	11
2.4 Shock Cord Design . . . . .	11
2.4.1 Parachute Opening Shock Force . . . . .	12
2.4.2 Rocket Mass . . . . .	12
2.4.3 Deployment Velocity and Dynamic Pressure . . . . .	12
2.4.4 Parachute Size and Drag Coefficient . . . . .	13
2.4.5 Inflation Time and Canopy Fill Constant . . . . .	13
2.4.6 Force Reduction Factor $X_1$ . . . . .	14
2.4.7 Empirical Opening Force Coefficient . . . . .	15
2.5 Ejection Mechanisms . . . . .	17
2.5.1 Pyrotechnic Charges . . . . .	17
2.5.2 Spring-based Systems . . . . .	19
2.6 Avionics and Sensors . . . . .	20

2.6.1	Flight Software Implementation . . . . .	20
2.7	Filtering Algorithms . . . . .	21
2.7.1	2D Kalman Filter . . . . .	22
2.7.2	Extended Kalman Filter (EKF) . . . . .	23
2.7.3	Particle Filter (PF) . . . . .	24
2.7.4	Key Differences . . . . .	24
2.7.5	Telemetry . . . . .	25
2.8	Research Gaps . . . . .	25
<b>3</b>	<b>Methodology . . . . .</b>	<b>27</b>
3.1	Mechanical Module . . . . .	27
3.1.1	Mechanical Design Considerations . . . . .	27
3.1.2	Drogue Parachute and Main Parachute Sub-assemblies . . . . .	27
3.1.3	Avionics Bay Subassembly . . . . .	31
3.1.4	Shear Pin Selection . . . . .	33
3.1.5	Ejection Charge Calculations . . . . .	34
3.1.6	Eyebolt Selection . . . . .	37
3.1.7	Bulkhead Screws Design . . . . .	38
3.2	Electrical Design . . . . .	39
3.2.1	Design considerations for the electrical module . . . . .	40
3.2.2	Sensors . . . . .	41
3.2.3	Telemetry . . . . .	43
3.2.4	Flight Computer Power Requirements . . . . .	45
3.2.5	Telemetry . . . . .	49
3.3	Software Design . . . . .	50
3.3.1	Design Considerations . . . . .	50
3.3.2	Kalman Filter Algorithm . . . . .	51
3.3.3	State Machine . . . . .	52
3.3.4	Variables . . . . .	53
3.3.5	User Interface . . . . .	54

<b>4 Results and Discussion . . . . .</b>	<b>57</b>
4.1 Main and Drogue Parachute . . . . .	57
4.2 Avionics Bay . . . . .	60
4.3 Eye Bolt . . . . .	62
4.4 Control Flowchart . . . . .	64
4.5 Control and Software Module . . . . .	65
4.6 User Interface . . . . .	67
<b>5 Summary, Conclusion, and Future Work . . . . .</b>	<b>71</b>
<b>References . . . . .</b>	<b>72</b>
<b>A Appendix . . . . .</b>	<b>75</b>
A.1 Time plan . . . . .	75
A.2 Budget . . . . .	76
A.3 Production Plan . . . . .	77
A.4 Design Drawings . . . . .	78

## List of Figures

Figure 2.1 A high-power rocket utilizing a single recovery system. . . . .	5
Figure 2.2 Comparison of drift between a single and a dual recovery system . . . . .	6
Figure 2.3 A high-power rocket utilizing a dual recovery system. . . . .	8
Figure 2.4 Relationship between Ballistic Parameter and force reduction factor .	15
Figure 2.5 Empirical opening force coefficient chart . . . . .	16
Figure 2.6 Diagram of pyrotechnic ejection sequence . . . . .	18
Figure 2.7 Image of a spring based ejection system Image source . . . . .	20
Figure 2.8 Example of avionics system in a rocket. Image source . . . . .	21
Figure 3.1 Components of a parachute system Image source . . . . .	29
Figure 3.2 Components of a parachute system Image source . . . . .	29
Figure 3.3 Components of a parachute system Image source . . . . .	30
Figure 3.4 Avionics Bay Sub-assembly . . . . .	31
Figure 3.5 Dual recovery system electrical block diagram . . . . .	40
Figure 3.6 MPU-6050 sensor connection to ESP-32 . . . . .	41
Figure 3.7 GPS sensor connection to ESP-32 . . . . .	42
Figure 3.8 BMP-180 module connection to ESP-32 . . . . .	43
Figure 3.9 SD card module connection to ESP-32 . . . . .	44
Figure 3.10Lora module connection to ESP-32 . . . . .	44
Figure 3.11A model of the ignition circuit in Proteus . . . . .	46
Figure 3.12Flight computer schematic . . . . .	48
Figure 3.13Flight computer PCB . . . . .	49
Figure 4.1 Assembly drawing of the drogue parachute . . . . .	57
Figure 4.2 Fabricated drogue parachute . . . . .	58
Figure 4.3 main chute . . . . .	59
Figure 4.4 Fabricated main parachute . . . . .	60
Figure 4.5 3D model of the avionics bay . . . . .	61
Figure 4.6 avionics bay model . . . . .	61
Figure 4.7 Fabricated avionics bay . . . . .	62

Figure 4.8 drogue chute . . . . .	63
Figure 4.9 User Interface Main Dashboard Panel . . . . .	68
Figure 4.10 Apogee threshold panel . . . . .	69
Figure 4.11 User Interface mobile view . . . . .	70
Figure A.1 Time plan . . . . .	75
Figure A.2 main parachute . . . . .	78
Figure A.3 drogue chute . . . . .	78
Figure A.4 avionics bay sub assembly . . . . .	79
Figure A.5 avionics bay lid . . . . .	79
Figure A.6 avionics bay protector . . . . .	80
Figure A.7 bulkhead . . . . .	80
Figure A.8 charge holder . . . . .	81
Figure A.9 eye bolt . . . . .	81
Figure A.10 shear pin . . . . .	82
Figure A.11 Avionics Bay Assembly . . . . .	82

## List of Tables

Table 2.1	Types of parachutes and their characteristics . . . . .	9
Table 2.2	Comparison of Materials . . . . .	11
Table 2.3	Comparison of communication modules for telemetry in amateur rocketry . . . . .	25
Table 2.4	Comparison between Nakuja N3.5 group's implementation and research gaps . . . . .	26
Table 3.1	Design Considerations for Ejection Charge . . . . .	35
Table 3.2	Power Requirements for Sensors . . . . .	45
Table 3.3	Power Requirements for Telemetry Components . . . . .	45
Table 3.4	Power Requirements for Ejection System . . . . .	46
Table 4.1	Shock Cord Material Selection . . . . .	62
Table 4.2	Selection of shock cord width . . . . .	62
Table 4.3	Measured Metrics . . . . .	66
Table A.1	Budget for Items . . . . .	76
Table A.2	Project Plan . . . . .	77

# 1 Introduction

The dual deployment parachute recovery system has become an essential technique in high-power rocketry, providing enhanced safety and precision during descent. Initially, rocket recovery relied on single parachute systems, which often resulted in uncontrolled, hard landings that could damage both the rocket and its surroundings[1, 2]. In the 1980s, amateur rocketry groups began experimenting with dual deployment to address these issues, aiming to improve recovery accuracy and minimize drift caused by winds during descent. This innovation was driven by the need for safer landings, especially as rockets became more powerful and valuable.[1, 2]

The dual deployment system involves two parachutes: a drogue chute and a main chute, each deployed at different stages of descent to achieve controlled landings [1, 2]. The drogue chute deploys at apogee to stabilize the rocket and slow its descent without arresting it completely, preventing excessive tumbling [3]. Later, as the rocket nears the ground, the main parachute deploys to provide a gentle, controlled landing near the launch point [4]. This technique became widely adopted in the 1990s, especially within high-power rocketry, due to its effectiveness in ensuring safe and predictable recoveries.

Our project focuses on designing, implementing, and validating a dual deployment system, with the goal of ensuring reliable recovery and reducing drift, which is critical for maintaining safety and efficiency in high-power rocket operations [5].

## 1.1 Problem Statement:

In high-power rocketry, deploying the main parachute at a high altitude apogee results in excessive drift and a significantly slower descent. Consequently, the rocket often lands much further away from the launch point than desired. This extended drift makes tracking and recovering the rocket particularly challenging and time-consuming, especially when the landing site is in rough or inaccessible terrain. The increased distance and difficulty in recovery not only add to the operational complexity but also heighten the risk of losing valuable rocket components.

## 1.2 Objectives

### 1.2.1 Main Objective:

To design and fabricate a dual deployment parachute recovery system for the N4 rocket.

### 1.2.2 Specific Objectives:

The specific objectives of this project are as follows:

1. To design and fabricate the mechanical structure of the dual event ejection mechanism including the main and the drogue parachute.
2. To develop a fully functional flight computer with electronic circuitry, incorporating sensors for altitude, acceleration, position, orientation, and a communication module to the base station.
3. To develop a state machine using a filtering algorithm to detect apogee and determine the precise moments for drogue and main parachute deployment.
4. To integrate all the components into a functional dual recovery system.

## 1.3 Scope

The scope of this project encompasses the design and fabrication of a dual event ejection mechanism, which includes creating both the mechanical structure and the main and drogue parachutes. Additionally, the project involves developing a fully functional flight computer with integrated electronic circuitry and sensors for altitude, acceleration, position, and orientation, alongside a communication module for real-time data transmission to a base station. A key component of the project is the development of a state machine using a filtering algorithm to accurately detect the rocket's apogee and determine the precise moments for deploying the drogue and main parachutes. Finally, all these components will be integrated into a cohesive and operational dual recovery system, ensuring the rocket's safe and controlled descent.

## 1.4 Justification:

Recovering rockets after high-altitude ejections presents significant challenges due to wind drift, which can cause rockets to land far from the intended recovery zone, complicating and prolonging the recovery process. This can be particularly problematic in rough or inaccessible terrains, making it difficult to locate and retrieve the rocket promptly. By implementing a dual-recovery system, which employs both a drogue and a main parachute, we can substantially mitigate these issues. The drogue parachute deploys at apogee, stabilizing and slowing the descent without fully arresting it, while the main parachute deploys at a lower altitude, ensuring a slower, controlled descent and reducing horizontal drift. This system enhances safety by minimizing the risk of damage during landing and increases efficiency by ensuring the rocket lands closer to the launch point. Consequently, the dual-recovery system not only facilitates quicker and more predictable recoveries but also boosts the overall success rate of missions by reducing the likelihood of loss or damage to the rocket.

## 2 Literature Review

### 2.1 History of Dual Recovery Systems

The history of dual recovery systems in rocketry began in the late 20th century, driven by the need for safer and more controlled recoveries in high-power and experimental rocketry. Initially, single parachute deployments were used, but they proved inadequate for high-altitude flights due to high descent speeds and significant drift. The figure below shows a single parachute deployment system used by Estes model rockets.

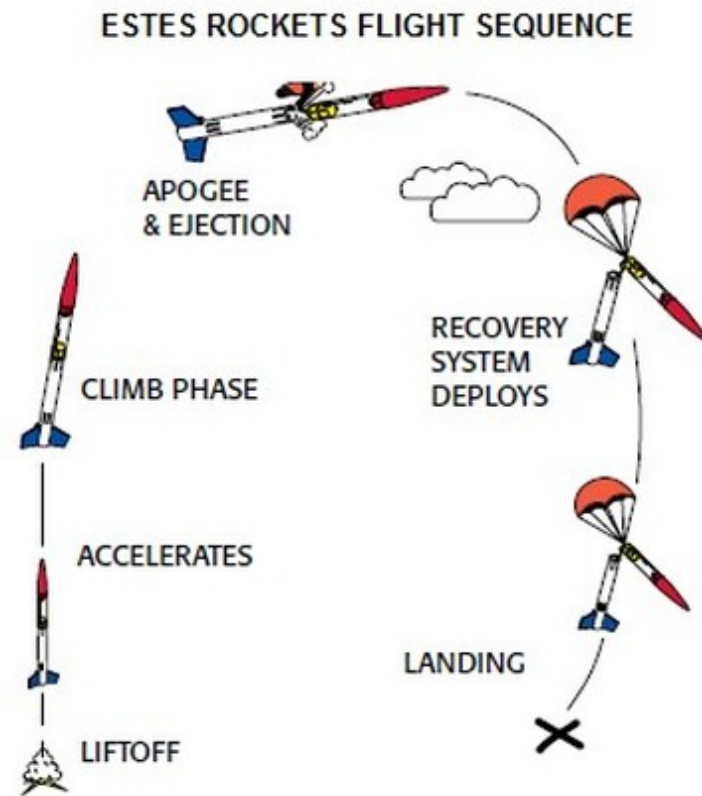


Figure 2.1: A high-power rocket utilizing a single recovery system.

In the 1980s and 1990s, pioneers in the field, supported by organizations like the Tripoli Rocketry Association and the National Association of Rocketry, started developing two-stage parachute systems [6]. The advent of reliable altimeters and flight computers allowed precise control over the timing of drogue and main parachute deployments, reducing descent speeds and improving landing accuracy [7].

By the 1990s and early 2000s, dual recovery systems had gained widespread acceptance thanks to advances in affordable electronics and growing recognition of their benefits in competitions and high-altitude flights [8]. Modern iterations have integrated advanced sensors, GPS technology, and real-time data logging, enhancing their accuracy and reliability [9]. Today, dual event ejection systems are standard in high-power rocketry, ensuring safe and predictable recoveries and supporting ongoing innovation in the field [10].

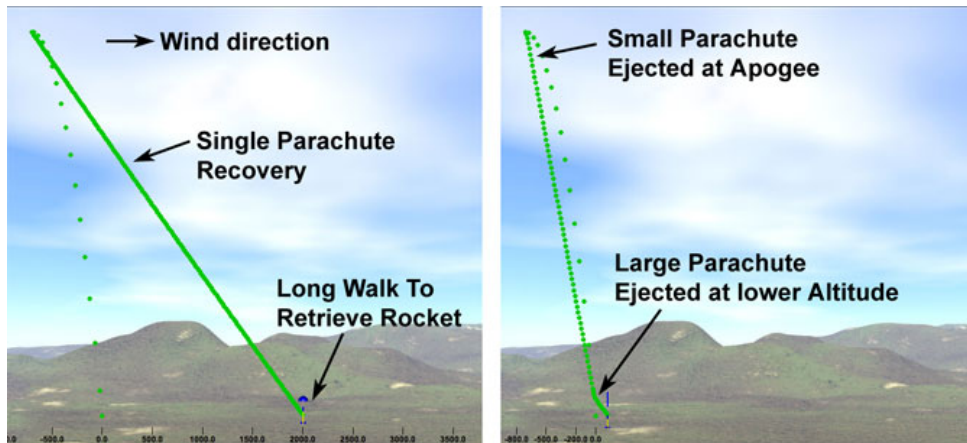


Figure 2.2: Comparison of drift between a single and a dual recovery system

## 2.2 Operation Sequence

The operation sequence in dual recovery systems involves multiple stages to ensure a controlled descent. In rockets developed by BPS Space and the TRA, the sequence begins at apogee, where an onboard altimeter, such as the PerfectFlite Stratologger CF, detects the highest point of the rocket's flight. At this point, a signal is sent to deploy the drogue

parachute. The drogue parachute stabilizes the rocket and slows its descent, reducing terminal velocity to a manageable level and preventing excessive drift caused by high-altitude winds [11].

As the rocket continues its descent, a second altitude threshold is reached, typically between 500 to 1,000 feet above ground level. The altimeter or a separate barometric sensor, such as the Altus Metrum TeleMega, triggers the deployment of the main parachute. The main parachute significantly increases drag, further slowing the descent to ensure a soft landing. This two-stage recovery process reduces the risk of damage to the rocket and its payload, allowing for safe retrieval and reuse [12].



Figure 2.3: A high-power rocket utilizing a dual recovery system.

## 2.3 Comparison of Parachute Types

Table 2.1: Types of parachutes and their characteristics

Parachute Type	Drag Coefficient (Cd)	Descent Stability	Ease of Fabrication	Image
Hemispherical	1.3 - 1.5	High, tends to be stable with minimal oscillation	Moderate, relatively simple pattern and assembly	
Circular	0.75 - 1.2	Moderate, can oscillate if not reefed or vented	Simple, basic design and straightforward assembly	
Elliptical	1.0 - 1.3	High, more stable descent due to shape	Complex, requires precise cutting and sewing	
Toroidal	0.8 - 1.0	High, excellent stability due to aerodynamic shape	Complex, involves intricate design and assembly	

Table 2.1 compares parachute types, emphasizing the trade-offs between stability, drag efficiency, and fabrication complexity. Hemispherical and elliptical parachutes provide high stability, but elliptical designs are more complex. Circular parachutes are simpler but may lack stability. Toroidal parachutes offer excellent stability but are the most intricate to fabricate. The choice of parachute depends on balancing performance needs with ease of construction.

### 2.3.1 Parachute Design and Sizing

Parachute size is determined by the mass of the rocket, desired descent rate, and drag characteristics of the parachute. The calculation is a two-step process. First, the area,  $A$ , of the parachute is calculated using equation 2.1[13]

$$A = \frac{2mg}{\rho v_T^2 C_D} \quad (2.1)$$

where

- $m$  = mass of the rocket,
- $v_T$  = desired terminal velocity,
- $C_D$  = drag coefficient of the parachute,
- $\rho = 1.22 \text{ kg/m}^3$  = air density at sea level at 15°C,
- $g = 9.807 \text{ m/s}^2$  = acceleration due to gravity.

The diameter is then calculated from the surface area based on the shape:- For hexagonal parachutes, the diameter,  $D$ , can be calculated as shown in equation (2.2), while for square parachutes, the length of each side,  $L$ , is calculated using equation (2.3). For all other parachutes, the shape is assumed to be circular and the diameter is calculated using equation (2.4).[14]

$$D = \sqrt{\frac{2A}{\sqrt{3}}} \quad (2.2)$$

$$L = \sqrt{A} \quad (2.3)$$

$$D = \sqrt{\frac{4A}{\pi}} \quad (2.4)$$

### 2.3.2 Materials Used in Parachute Fabrication

The selection of materials for parachute fabrication is critical to ensure reliability and performance. The common materials used are summarized in table 2.2[15]

Table 2.2: Comparison of Materials

Material	Advantages	Disadvantages
Ripstop Nylon	<ul style="list-style-type: none"> <li>- Lightweight.</li> <li>- High tear resistance.</li> <li>- Low porosity, reducing air leakage.</li> </ul>	<ul style="list-style-type: none"> <li>- Can degrade under prolonged UV exposure.</li> <li>- Less flexible compared to other fabrics.</li> </ul>
Silk	<ul style="list-style-type: none"> <li>- Very lightweight and strong.</li> <li>- Smooth texture reduces air drag.</li> </ul>	<ul style="list-style-type: none"> <li>- Prone to UV damage.</li> <li>- Higher cost compared to synthetic fabrics.</li> </ul>
Kevlar	<ul style="list-style-type: none"> <li>- High strength-to-weight ratio.</li> <li>- Excellent thermal stability.</li> </ul>	<ul style="list-style-type: none"> <li>- Expensive material.</li> <li>- Difficult to sew and fabricate.</li> </ul>

## 2.4 Shock Cord Design

The design of the shock cord is critical in ensuring the safe deployment of the parachute and the protection of the rocket from the forces experienced during deployment. A key aspect of the shock cord design is the estimation of the parachute opening shock force, which is influenced by factors such as the rocket's mass, the deployment velocity, parachute size, and atmospheric conditions.

### 2.4.1 Parachute Opening Shock Force

The parachute opening shock force can be estimated using the Pflanz Method, which combines empirical and semi-empirical models to calculate the peak force generated during parachute deployment. The equation for the parachute opening shock force is expressed as:

$$F_x = (S \cdot C_D)_p \cdot q \cdot C_x \cdot X_1 \quad (2.5)$$

where  $F_x$  is the parachute opening shock force,  $(S \cdot C_D)_p$  represents the product of the parachute surface area and drag coefficient,  $q$  is the dynamic pressure,  $C_x$  is the empirical opening force coefficient, and  $X_1$  is the force reduction factor, which is based on the ballistic parameter  $A$ .

### 2.4.2 Rocket Mass

The mass of the rocket, denoted by  $m$ , plays a significant role in determining the total gravitational force  $W_t$ , which contributes to the opening shock force. The gravitational force is given by the equation:

$$W_t = m \cdot g \quad (2.6)$$

where  $g$  is the acceleration due to gravity. The mass of the rocket directly influences the force experienced by the shock cord during parachute deployment.

### 2.4.3 Deployment Velocity and Dynamic Pressure

The deployment velocity,  $v_t$ , of the parachute is another critical factor influencing the dynamic pressure  $q$ , which is used in the Pflanz Method. The dynamic pressure can be calculated using the following equation:

$$q = \frac{1}{2} \cdot \rho \cdot v_t^2 \quad (2.7)$$

where  $\rho$  is the air density and  $v_t$  is the velocity at which the parachute is deployed. The dynamic pressure is a key parameter in determining the magnitude of the opening shock force.

#### 2.4.4 Parachute Size and Drag Coefficient

The effective drag area,  $(S \cdot C_D)_p$ , is calculated by multiplying the surface area of the parachute  $S$  and the drag coefficient  $C_D$ . The surface area of the parachute is calculated using the equation:

$$S = \pi \cdot \left(\frac{D}{2}\right)^2 \quad (2.8)$$

where  $D$  is the parachute diameter. The drag coefficient  $C_D$  is determined based on the parachute's design and performance characteristics. These two parameters are used to estimate the drag force acting on the parachute during deployment.

#### 2.4.5 Inflation Time and Canopy Fill Constant

The inflation time of the parachute,  $t_f$ , is an important factor in determining how quickly the parachute fills and begins to exert force on the shock cord. The inflation time is calculated using the canopy fill constant  $n$  and the parachute diameter  $D_0$  with the following equation:

$$t_f = \frac{n \cdot D_0}{v_t} \quad (2.9)$$

where  $n$  is a constant that depends on the specific parachute design. The inflation time affects the rate at which the parachute deploys and is critical for determining the forces experienced during deployment.

### Ballistic Parameter $A$

The ballistic parameter  $A$  is another key factor that influences the parachute opening shock force. It is calculated using the following equation:

$$A = \frac{2 \cdot W_t}{(S \cdot C_D)_p \cdot \rho \cdot g \cdot v_1 \cdot t_f} \quad (2.10)$$

where  $W_t$  is the total weight of the rocket,  $(S \cdot C_D)_p$  is the effective drag area,  $\rho$  is the air density,  $g$  is the acceleration due to gravity,  $v_1$  is the velocity at which the parachute starts to deploy, and  $t_f$  is the inflation time.

#### 2.4.6 Force Reduction Factor $X_1$

The force reduction factor,  $X_1$ , is derived from empirical data and is used to account for the reduction in the opening shock force due to factors such as the parachute's inflation characteristics. It is typically determined from charts based on the ballistic parameter  $A$ . The force reduction factor is a critical factor in accurately estimating the parachute opening shock force.

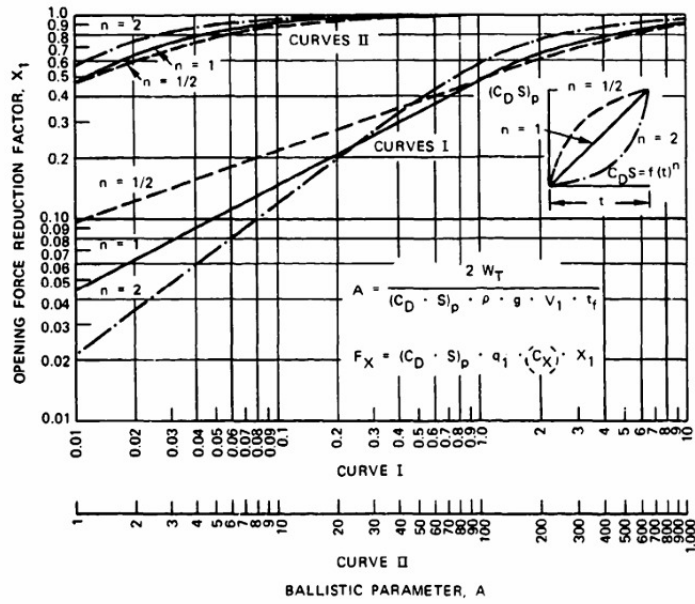


Figure 2.4: Relationship between Ballistic Parameter and force reduction factor

#### 2.4.7 Empirical Opening Force Coefficient

The empirical opening force coefficient  $C_x$  is used in the Pflanz Method to account for the characteristics of the parachute opening. This coefficient is typically derived from experimental data and is a function of various factors such as parachute size, deployment velocity, and atmospheric conditions. The value of  $C_x$  can be obtained from charts or empirical formulas based on the specific parachute design.

TABLE 5-1. Solid Textile Parachutes.

TYPE	CONSTRUCTED SHAPE PLAN PROFILE	$\frac{D_c}{D_o}$	INFLATED SHAPE $\frac{D_p}{D_o}$	DRAg COEF $C_{D_o}$ RANGE	OPENING FORCE COEF $C_x$ (INF MASS)	AVERAGE ANGLE OF OSCILLATION, DEGREES	GENERAL APPLICATION
FLAT CIRCULAR		—	1.00	0.67 TO 0.70	0.75 TO 0.80	~1.7	±10 TO ±40 DESCENT, OBSOLETE
CONICAL		0.93 TO 0.95	0.70	0.75 TO 0.90	~1.8	±10 TO ±30	DESCENT, M < 0.5
BICONICAL		0.90 TO 0.95	0.70	0.75 TO 0.92	~1.8	±10 TO ±30	DESCENT, M < 0.5
TRICONICAL POLYCONICAL		0.90 TO 0.95	0.70	0.80 TO 0.96	~1.8	±10 TO ±20	DESCENT, M < 0.5
EXTENDED SKIRT 10% FLAT		0.86	0.66 TO 0.70	0.78 TO 0.87	~1.4	±10 TO ±15	DESCENT, M < 0.5
EXTENDED SKIRT 14 3/4% FULL		0.81 TO 0.85	0.66 TO 0.70	0.75 TO 0.90	~1.4	±10 TO ±15	DESCENT, M < 0.5
HEMISPHERICAL		0.71	0.66	0.62 TO 0.77	~1.6	±10 TO ±15	DESCENT, M < 0.5, OBSOLETE
GUIDE SURFACE (RIBBED)		0.63	0.62	0.28 TO 0.42	~1.2	0 TO -2	STABILIZATION, DROGUE, 0.1 < M < 1.5
GUIDE SURFACE (RIBLESS)		0.66	0.63	0.30 TO 0.34	~1.4	0 TO -3	PILOT, DROGUE, 0.1 < M < 1.5
ANNULAR		1.04	0.94	0.85 TO 0.95	~1.4	< -6	DESCENT, M < 0.5
CROSS		1.15 TO 1.19	0.65 TO 0.72	0.60 TO 0.85	1.1 TO 1.2	0 TO -3	DESCENT, DECELERATION

Figure 2.5: Empirical opening force coefficient chart

In summary, the design of the shock cord requires careful consideration of several parameters, including the rocket's mass, deployment velocity, parachute size, drag coefficient, inflation time, and force reduction factors. By using the Pflanz Method, it is possible to estimate the parachute opening shock force and design the shock cord to withstand these forces, ensuring safe and reliable parachute deployment.

## 2.5 Ejection Mechanisms

Ejection mechanisms in rocketry are designed to deploy recovery devices, such as parachutes, at specific points during the rocket's descent. They typically use small explosive charges or pressurized systems to forcibly separate sections of the rocket, allowing the parachutes to deploy and slow the rocket's descent for a safe landing.

### 2.5.1 Pyrotechnic Charges

Pyrotechnic charges are widely used for their reliability and ability to function under extreme conditions. These charges consist of small explosive devices that, when ignited, rapidly expand gases to forcefully eject the parachute. The explosive charges commonly used are black powder and crimson powder. Black powder, also known as gunpowder, is a well-known propellant composed of potassium nitrate ( $\text{KNO}_3$ ), charcoal (C), and sulfur (S). The simplified chemical reaction for the combustion of black powder is:

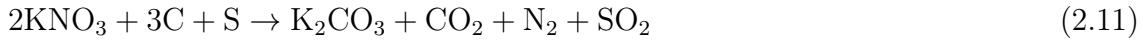




Figure 2.6: Diagram of pyrotechnic ejection sequence

The gases produced by the combustion process rapidly expand, exerting pressure on the surrounding components, resulting in the deployment of the parachute [16]. The pressure required for ejection is determined by the desired force, or alternatively, the force can be set by specifying the desired pressure. This relationship is given by equation(2.6).

$$P = \frac{F}{\pi \left(\frac{D}{2}\right)^2} \quad (2.12)$$

where:

- $F$  = Desired force
- $D$  = Body tube diameter

Once the desired pressure  $P$  is known, the amount of black powder required can be calculated using equation(2.7).

$$m = \frac{PV}{R_c T g} \quad (2.13)$$

where:

- $P$  = Pressure calculated from the previous equation
- $V$  = Volume of the chamber to be pressurized
- $R_c = 12.1579 \frac{m}{K}$  (combustion gas constant for FFFFg black powder)
- $T = 1739 K$  (combustion gas temperature)
- $g = 9.807 \frac{m}{s^2}$  (acceleration due to gravity) [17]

### 2.5.2 Spring-based Systems

Spring-based ejection systems, shown in figure 2.5, offer a mechanical alternative to pyrotechnic charges. These systems rely on the potential energy stored in compressed springs to deploy parachutes. When triggered, the springs release their energy, pushing out the parachute. This method is particularly useful in environments where pyrotechnics are not allowed or are deemed unsafe. Spring-based systems are more complex to design but offer reliable performance with fewer safety concerns [18].

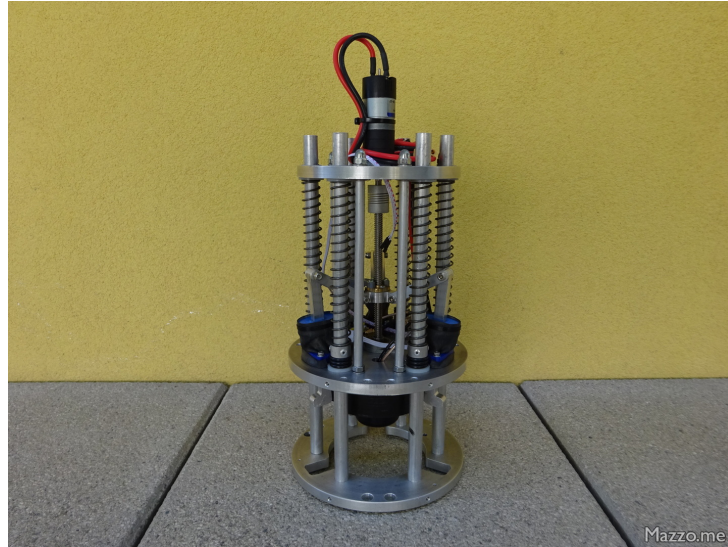


Figure 2.7: Image of a spring based ejection system Image source

## 2.6 Avionics and Sensors

Avionics in dual recovery systems include altimeters, barometric pressure sensors, accelerometers, and gyroscopes. These components work together to determine the rocket's position, speed, and altitude. The altimeter is the primary sensor, typically measuring changes in atmospheric pressure to determine altitude. Accelerometers measure the rocket's acceleration during ascent and descent, while gyroscopes provide data on orientation and stability [7].

### 2.6.1 Flight Software Implementation

The flight software in dual recovery systems is essential for processing avionics data and managing parachute deployments. Typically written in C++ or Python, this software handles several critical tasks:

- **Apogee Detection:** Algorithms process sensor data to accurately determine the rocket's apogee, ensuring timely deployment of recovery systems [19].
- **Ejection Control:** The software controls the deployment sequence of parachutes based on apogee detection and flight parameters [20].

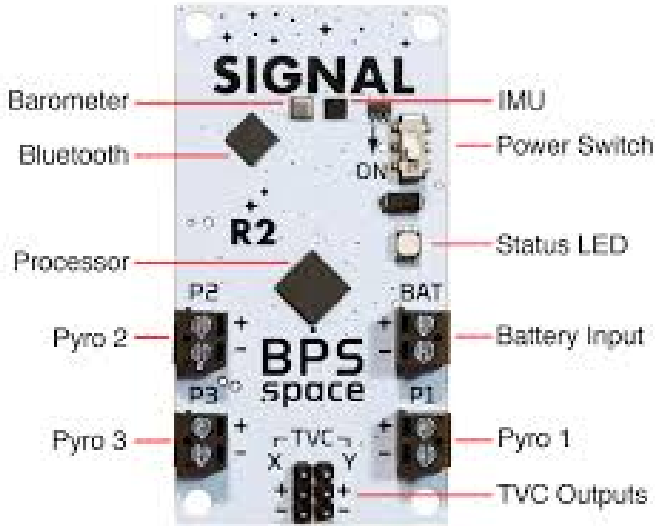


Figure 2.8: Example of avionics system in a rocket. Image source

- **Data Logging and Telemetry:** It logs flight data and transmits it to ground stations, providing real-time monitoring and post-flight analysis [21].
- **Safety Checks:** Redundancy and safety checks are implemented to minimize the risk of failure and ensure reliable operation [22].

The software used by organizations like the Tripoli Rocketry Association (TRA) exemplifies these principles by integrating multiple sensor inputs to enhance accuracy and reliability [23].

## 2.7 Filtering Algorithms

In high-power rocketry, accurately estimating a rocket's position, velocity, and other dynamic states in real time is essential for recovery. Due to the noisy nature of sensor data and the complex, nonlinear behavior of the rocket's flight, advanced filtering algorithms are required to extract meaningful estimates from noisy measurements. This section examines three key filtering techniques commonly used in high-power rocketry: the 2D Kalman Filter, the Extended Kalman Filter (EKF), and the Particle Filter (PF). The 2D

Kalman Filter is well-suited for linear flight dynamics but struggles with the nonlinearities typical in rocket trajectories [24]. The EKF addresses this by linearizing the system around current estimates, making it more applicable to the non-linear environment of a rocket's flight [25]. For even more complex scenarios involving highly nonlinear dynamics and non-Gaussian noise, the Particle Filter offers a more robust solution by approximating the rocket's state using a set of weighted particles [26]. These filters play a crucial role in ensuring the accuracy and reliability of onboard state estimation throughout the rocket's flight phases.

### 2.7.1 2D Kalman Filter

The 2D Kalman Filter extends the traditional Kalman Filter to estimate the state of a system in two dimensions, such as position and velocity, based on noisy measurements. It iteratively updates the state estimate and the associated uncertainty by incorporating new measurements. The filter follows three key equations:

$$\hat{x}_k = \hat{x}_{k-1} + K_k (z_k - H\hat{x}_{k-1}) \quad (2.14)$$

This equation updates the state estimate  $\hat{x}_k$ , where  $\hat{x}_{k-1}$  is the previous estimate,  $z_k$  is the new measurement, and  $H$  is the measurement matrix that relates the state to the measurement. The term  $K_k$  represents the Kalman Gain, which determines how much the measurement influences the update [24].

$$P_k = (I - K_k H)P_{k-1} \quad (2.15)$$

This equation updates the uncertainty (covariance matrix)  $P_k$ , accounting for how much the new measurement reduces the overall uncertainty.  $I$  is the identity matrix, and  $K_k$  is the Kalman Gain, which reduces the uncertainty based on the reliability of the measurement.

$$K_k = \frac{P_{k-1}H^T}{HP_{k-1}H^T + R} \quad (2.16)$$

The Kalman Gain  $K_k$  is calculated based on the previous uncertainty  $P_{k-1}$ , the measurement matrix  $H$ , and the measurement noise covariance  $R$ . It balances the weight given to the new measurement against the current state estimate's uncertainty.

The 2D Kalman Filter differs from the 1D version by estimating two interrelated state variables (e.g., position and velocity), instead of one, and updating the state and uncertainty in both dimensions simultaneously. This allows it to handle more complex systems like those in high-power rocketry, where both position and velocity change dynamically during flight [27].

### 2.7.2 Extended Kalman Filter (EKF)

The Extended Kalman Filter is an extension of the 2D Kalman Filter that handles non-linear systems by linearizing them around the current estimate. The EKF updates the state estimate using:

$$\hat{x}_k = \hat{x}_{k-1} + K_k (z_k - h(\hat{x}_{k-1})) \quad (2.17)$$

$$P_k = (I - K_k H_k) P_{k-1} \quad (2.18)$$

$$K_k = \frac{P_{k-1}H_k^T}{H_k P_{k-1} H_k^T + R} \quad (2.19)$$

where: -  $h(\hat{x}_{k-1})$  = nonlinear measurement function -  $H_k$  = Jacobian matrix of  $h(\hat{x}_{k-1})$

### 2.7.3 Particle Filter (PF)

The Particle Filter estimates the state of a system using a set of particles, each representing a possible state. It updates the particles and their associated weights based on the likelihood of the measurement given each particle's state. The state estimate is computed as the weighted average of the particles [26].

$$\hat{x}_k = \sum_{i=1}^N w_k^{(i)} x_k^{(i)} \quad (2.20)$$

where: -  $x_k^{(i)}$  = state of the  $i$ -th particle at time  $k$  -  $w_k^{(i)}$  = weight of the  $i$ -th particle at time  $k$  -  $N$  = number of particles

### 2.7.4 Key Differences

- **System Type:** The 2D Kalman Filter is best suited for linear systems, while the EKF can handle nonlinear systems by linearizing them. The Particle Filter can handle highly nonlinear and non-Gaussian systems without the need for linearization [26].
- **Complexity:** The 2D Kalman Filter and EKF are computationally efficient due to their recursive nature. The Particle Filter is more computationally intensive as it involves simulating multiple particles and resampling them at each step.
- **Estimation Accuracy:** The Particle Filter provides more accurate estimates in complex scenarios with non-linearities and non-Gaussian noise, while the EKF may struggle with significant non-linearities. The 2D Kalman Filter is precise for linear systems but not suitable for non-linear systems [24].

### 2.7.5 Telemetry

Table 2.3 presents a comparison of different communication modules available for high-power rocketry.

Table 2.3: Comparison of communication modules for telemetry in amateur rocketry

Parameter	Digi XBee-PRO 900HP	LoRa	Wi-Fi (ESP32)
Bandwidth	200 kbps	37.5 kbps	54 Mbps (802.11g), 150 Mbps (802.11n)
Range	Up to 45 km (line of sight)	Up to 15-20 km (line of sight)	Up to 200 meters (line of sight)
Power Consumption	250 mW (transmit), 0.5 mW (sleep)	10-50 mW (transmit), <1 mW (sleep)	500 mW (transmit), 50 mW (idle), 2 mW (sleep)

BPS Space uses the 915 MHz LoRa transceiver for telemetry communication, which enables long-range, low-power data transmission. This module transmits data on altitude, speed, and parachute deployment status to ground control stations. Additionally, the use of a u-blox NEO-M8N GPS module provides real-time tracking of the rocket's location [26].

TRA rockets often use the XBee Pro 900HP for wireless data links, which supports robust communication over long distances. Real-time tracking capabilities are also provided by GPS modules, such as the u-blox NEO-M8N. These systems transmit continuous data streams on flight dynamics and recovery status, crucial for real-time decision-making and post-flight analysis [28].

## 2.8 Research Gaps

The previous generation of Nakuja rockets had a target altitude of 1.6km or less, therefore they utilized a single deployment system. With a much higher altitude target, the N4

rocket has to utilize a dual recovery system, hence new solutions and existing gaps in the single recovery system have to be addressed. The following gaps were identified from the previous recovery system designs.

Table 2.4: Comparison between Nakuja N3.5 group's implementation and research gaps

<b>Nakuja N3.5 Implementation</b>	<b>Research Gap</b>
The group used a one-dimensional Kalman filter for altitude estimation.	A 2D Kalman filter can combine both accelerometer and BMP data, providing more accurate and precise altitude estimation.
The avionics bay was used solely as a housing for electrical components.	Dual use of the avionics bay as a structural coupler can optimize space and reduce overall weight.
No real-time adaptive algorithms were implemented to handle unexpected flight anomalies.	Implementing real-time adaptive algorithms can improve flight reliability by adjusting for unexpected conditions.
Unreliable onboard data logging capabilities for post-flight analysis.	Enhanced onboard data logging can provide comprehensive post-flight data for more detailed analysis.

## 3 Methodology

This section shows the design process that was used in the implementation of this project. The main purpose of this system was to deploy the main and the drogue parachutes at the desired flight states of the rocket. The dual deployment system consists of three main parts, the mechanical module, the actuation module and the software and control module.

### 3.1 Mechanical Module

The mechanical module consists of three sub-assemblies: the main parachute, the avionics bay and the drogue parachute.

#### 3.1.1 Mechanical Design Considerations

1. The main parachute should provide a descent rate of 21m/s.
2. The drogue parachute should provide a descent rate of 5.5m/s
3. The avionics bay should be able to fit within the rocket's airframe and the flight computer should be able to fit within the avionics bay
4. The amounts of ejection charges should be sufficient to deploy the main and the drogue parachutes.

Mechanical design was performed using SolidWorks CAD software. From the models, drawings for the parts were generated.

#### 3.1.2 Drogue Parachute and Main Parachute Sub-assemblies

The following considerations were observed when designing the main and drogue parachutes.

- The recoverable mass of the rocket, from simulations by the N4 airframe team, was given as 20kg.

- The terminal velocity required for the drogue parachute, selected as 5.5m/s.
- The terminal velocity of the main parachute, selected as 21m/s.

Using the respective terminal velocities as well as the recoverable mass of the rocket, the drogue and main parachute areas were calculated using equation (2.1). The nominal area of the main parachute was calculated as  $6.87 \text{ m}^2$ . The nominal area of the drogue parachute was calculated as  $0.47 \text{ m}^2$ .

Their diameters were then calculated from the values of area using equation (2.4). The diameter of the main parachute was found to be 2.96m and that of the drogue parachute as 0.77m

The number of gores-the sections making up the complete hemispherical parachutes, were selected based on the standard for gore number based on Rocketman Enterprises-Which is 4 gores for a drogue chute and 8 gores for the main chute.

The spill hole or apex vent area, as per Rocketman Enterprises, is taken as 1% of the canopy area to minimize parachute oscillation, was calculated as:

$$\text{Drogue chute spill hole area} = 0.047 \text{ m}^2$$

The diameter of the spill hole from equation (2.4) was found to be:

$$D_2 = 0.24 \text{ m}$$

$$\text{Main parachute spill hole area} = 0.069 \text{ m}^2$$

The diameter of the spill hole from equation (2.4) was found to be:

$$D_2 = 0.30 \text{ m}$$

Originally, the material selected for fabrication of the parachutes was ripstop nylon, however, this material was not available in country. Therefore , regular nylon fabric was used to fabricate the parachutes.

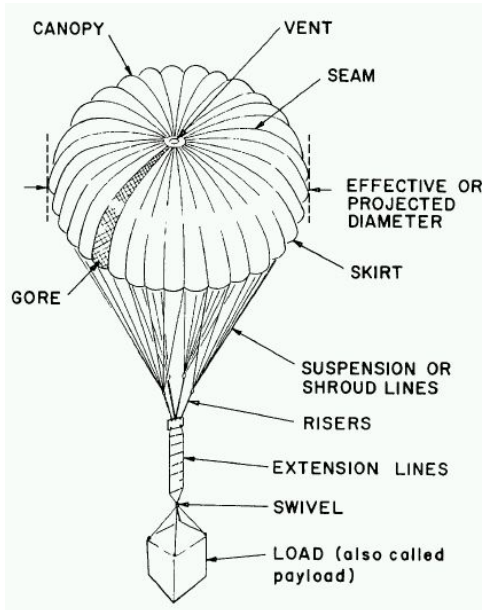


Figure 3.1: Components of a parachute system Image source

The dimensions as well as the gore numbers were sent to a tailor who determined the fabric dimensions from which the gores for each chute could be cut. The gores were then sewn together to form the complete parachutes. Shroud lines were then sewn onto every seam to help the parachutes form a canopy during inflation.

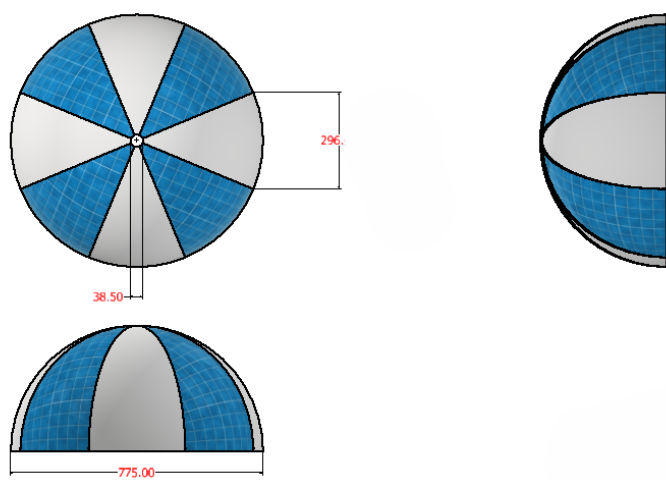


Figure 3.2: Components of a parachute system Image source

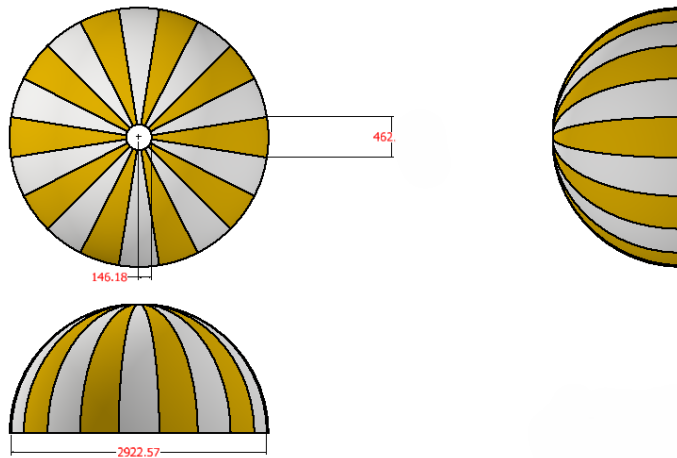


Figure 3.3: Components of a parachute system Image source

### Shock Cord Selection

The shock cord was designed to ensure safe and reliable parachute deployment while withstanding the forces experienced during the deployment phase. The primary goal was to design a shock cord capable of handling the parachute opening shock force, which was estimated using the Pflanz Method, as discussed in the literature review.

First, the parachute opening shock force was estimated by applying the Pflanz Method (Equation 2.5). Using the calculated values:

- The product of the parachute surface area and drag coefficient  $(S \cdot C_D)_p = 10.16 \text{ m}^2$ ,
- The dynamic pressure  $q = 270.11 \text{ Pa}$ , calculated from the deployment velocity  $v_t = 21 \text{ m/s}$  and air density  $\rho = 1.225 \text{ kg/m}^3$ ,
- The empirical opening force coefficient  $C_x = 1.2$ ,
- The force reduction factor  $X_1 = 0.99$ , based on the ballistic parameter  $A = 0.74$ .

Using these values, the parachute opening shock force was calculated to be approximately  $F_x = 4618 \text{ N}$ .

Additionally, the rocket's mass was  $m = 20\text{ kg}$ , resulting in a total gravitational force  $W_t = 196.2\text{ N}$  (Equation 3.3). The parachute diameter  $D = 2.9\text{ m}$  and the inflation time was calculated to be  $t_f = 0.207$  seconds, as described by Equation 2.9.

Based on these calculations, the shock cord was selected with a strength rating to withstand the parachute opening shock force of approximately  $F_x = 4618\text{ N}$ , ensuring that the parachute deployment would occur safely without failure of the shock cord. Kevlar was the material of choice for the shock cord, but its unavailability prompted the use of nylon rope of 6mm thickness as a replacement.

### 3.1.3 Avionics Bay Subassembly

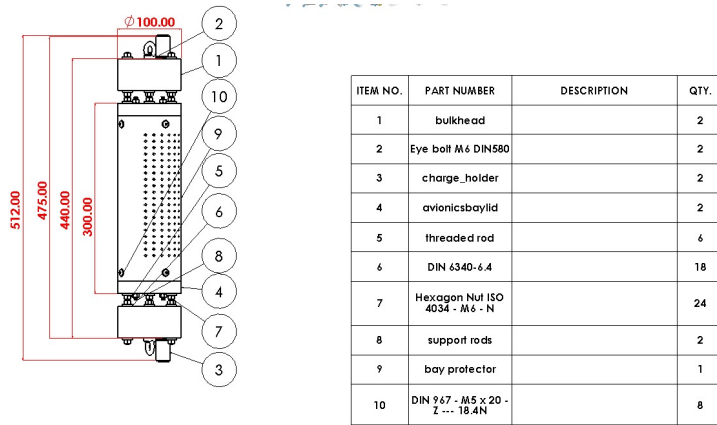


Figure 3.4: Avionics Bay Sub-assembly

The avionics bay assembly consists of bulkheads at each end made of soft nylon material. The bulkheads provide an attachment point for the charge holders into which the ejection charge is placed. Moreover, onto the bulkheads are attached the eyebolts [Part 2] ,made of stainless steel, which provide a tying point for the shock cords.

The avionics bay protector shields the electronic components from fast airflow let in through the vent holes. It has a matrix of holes that help to balance pressure within and outside the bay while preventing high air speeds inside the bay which could result in inaccurate altitude data from the BMP-180 barometric pressure sensor which relies on

air pressure measurement for altitude estimation.

The threaded rods are made of low carbon steel and are used to offer support to the avionics bay sub-assembly. At both ends of the flight computer holder are the avionics bay lids which ,together with the bay protector, enclose the flight computer holder.

### Fabrication and assembly of the Avionics Bay

The avionics bay bulkheads were fabricated as follows.

- Two cylindrical blocks of height 50 mm and diameter 101 mm were cut from a 500 mm soft nylon cylindrical bar using a hack saw.
- The two blocks were faced to a thickness of 30 mm using a three-jaw chuck on a center lathe to ensure flat and parallel surfaces.
- Each bulkhead was designed to contain three 6 mm holes for threaded rods and one 8 mm hole for an eye bolt. A drilling template, bearing the profiles of the required holes, was designed and 3D printed using a Prusa MK3S+ 3D printer.
- The drilling template was aligned with the bulkheads, and three 6 mm holes, spaced 120° apart on an 80 mm diameter construction circle, were drilled on a bench drilling press using a 6 mm drill bit. The central 8 mm hole for the eye bolt was drilled using an 8 mm drill bit.
- The lower bulkhead was turned from a diameter of 101 mm to 98 mm using a lathe to ensure a precise fit within the coupling, which has an internal diameter of 98 mm.

Following the bulkheads, two avionics bay lids were fabricated. The overall dimensions of the lids were 100mm diameter by 43mm thickness. The CAD model was converted to Standard Tessellation Language(STL) file format then loaded into the PrusaSlicer slicing software. Two instances of the model were set to be printed. The material used was PLA, from several printing tests performed on the filament, the optimum printing temperature was found to be 220 degrees celcius. The lids were printed with an infill density of 40

percent.

The third item to be fabricated was the avionics bay protector. Measuring 95.2mm diameter by 260mm in height and thickness of 2mm, it was too tall to be printed on the prusa MK3S+, therefore , it was printed using the Flsun QQS Pro 3D printer using the same settings as those of the avionics bay lid except for the infill density which was set to 80 percent to obtain a stronger part due to its small thickness.

Two charge holders,measuring 37mm in height, 18mm in internal diameter and 2mm thickness were also printed using the same setup as that of the avionics bay lids.

- The avionics bay lids, each with a thickness of 43 mm and a diameter of 100 mm,were sliced using .
- The flight computer holder, bay protector and charge cartridges were 3D printed using PLA material.
- Six threaded rod pieces, each 6 mm in diameter and 160 mm in length, were cut using a hack saw to secure the lids of the avionics bay to the bulkheads.
- Two support rods, each 320 mm in length and 6 mm in diameter, were fabricated to connect the two avionics bay lids and provide structural support to the flight computer holder.

**Changes to the avionics bay design** From figure 3.4, the space between the lower bulkhead and the lower avionics bay lid raised a concern of possible tilting of the upper section of the rocket which would cause air to gush into the rocket causing a launch failure. To solve this, a coupling was designed, which would be screwed onto the airframe and the lower bulkhead hence filling the gap.

### 3.1.4 Shear Pin Selection

Shear pins are mechanical components used to secure parts in place while allowing them to separate under a specified force. They are designed to shear off when a predetermined

load is exceeded, thus protecting other components from damage. In our design, the predetermined load for failure was chosen as 285N and 380N for the drogue and main parachute shear pins respectively. The number of shear pins to be used for the drogue and main parachutes were also selected intuitively as 4 and 3 respectively. This section outlines the calculations used to determine the appropriate diameter of shear pins for both the main and drogue parachutes.

### Design Considerations for Shear Pins

- Material: PLA. PLA was chosen because of its relatively low shear strength hence could shear off with less force and also result in a bigger shear pin diameter which would be easy to fabricate.
- Shear Strength:  $\tau = 26.77 \text{ MPa}$
- Main Parachute Shear Force:  $F_{\text{shear}} = 285 \text{ N}$ , Number of Pins:  $n = 3$
- Drogue Parachute Shear Force:  $F_{\text{shear}} = 380 \text{ N}$ , Number of Pins:  $n = 4$

The shear force to be withstood by the pins was given as:

$$P_s = \frac{\pi}{4} \times d^2 \times \tau \times n \quad (3.1)$$

Making  $d$  the subject of the formula and using the parameters provided above, the diameters for both the main and drogue parachutes were found to be approximately 2.126mm say 3mm using equation (3.8)

#### 3.1.5 Ejection Charge Calculations

Following the shock cord design, the next step was to calculate the ejection charges necessary to deploy the parachutes effectively. The amount of force required to break the shear pins and push out the parachute determined the amount of black powder charge to

be used. The distance the parachutes are to be thrown out also was selected intuitively as 4m and 2m. The force to overcome shear pins were taken from the shear pin discussion. The distance the parachutes were to be pushed by the ejection force is the distance from the bottom of the parachute bay to the nearest vent hole where the pressure producing the ejection force would be relieved. The diameter of the chamber was obtained from the N3.5 air-frame team. The height of the chamber was estimated using existing chamber allocations from the N3.5 recovery team. All these parameters are provided in table 3.1.

## Design Considerations

Table 3.1: Design Considerations for Ejection Charge

Parameter	Main Parachute	Drogue Chute
Mass of parachute, $m_p$	0.3 kg	0.3kg
Mass of nosecone, $m_n$	0.35 kg	0.35kg
Total mass, $m$	0.65 kg	4.78 kg
Distance to be thrown up by ejection force, $h$	4 m	2 m
Force to overcome shear pins, $F_{sp}$	285 N	380 N
Distance to push the parachute, $d$	0.2 m	0.2 m
Safety factor, $sf$	1.2	1.2
Diameter of chamber, $D$	0.1 m	0.1 m
Height of chamber, $h_c$	0.4 m	0.15 m
Gas constant for FFF black powder, $R_c$	265 J/(kg·K)	265 J/(kg·K)
Temperature, $T$	1739 K	1739 K
Acceleration due to gravity, $g$	9.81 m/s <sup>2</sup>	9.81 m/s <sup>2</sup>

## Calculations

The potential energy required to eject the parachutes was calculated using equation (3.2):

$$PE = mgh \quad (3.2)$$

Using equation (3.2), the potential energy required to push out the main and the drogue

parachutes to the required distances were found to be 25.5J and 93.7J respectively.

The force required to push the parachute was determined by dividing the potential energy by the distance over which it is applied:

$$F_p = \frac{PE}{d} \quad (3.3)$$

Using equation (3.3), the amount of force to push out the main and drogue parachutes were found to be 127.53 and 468.26N

The total force required to eject each parachute was calculated by adding the force to push the parachute and the force needed to overcome the shear pins. Moreover, a safety factor of 1.2 was applied to the resultant forces. Therefore, the forces required to eject the main and drogue parachutes were obtained as 495N and 1017N respectively.

The pressure needed in the chamber to achieve the required force was computed using the chamber's cross-sectional area, which was cylindrical in shape, using following equation:

$$A = \pi \left( \frac{D}{2} \right)^2 \quad (3.4)$$

The pressure required to provide the ejection force for the main parachute was calculated as 63101Pa while that required for the drogue parachute was found to be 129617Pa using equation (3.11).

The volume of the chamber was calculated to be used in determining the mass of black powder to be used using equation (3.5).

$$V_{\text{main}} = \pi \times \left( \frac{D}{2} \right)^2 \times h_c \quad (3.5)$$

From the dimensions provided in Table 3.1, the volume of the main chamber was obtained as 0.003 m<sup>3</sup> and that of the drogue chamber as 0.002 m<sup>3</sup>.

Finally, the mass of the ejection powder required was determined using the pressure, volume, and properties of the gas:

$$m = \frac{P \times V}{R_c \times T \times g} \quad (3.6)$$

Equation (3.6) yielded the mass of charge to eject both the main and drogue parachute as approximately 2 grams each using a safety factor of 2.

The initial charge estimation from the calculations was found to be 2 grams. During the first pop test, this amount was found to be insufficient in pushing out the nose-cone, moreover, black powder was found to be less potent than an alternative ejection charge-crimson powder. In pop test 2, 15 grams of crimson powder was used and ejection of the main parachute was successful.

### 3.1.6 Eyebolt Selection

The eye bolt is the component on to which the shock cord is tied so that it attaches the parachute to the rocket. The eye bolt was designed to withstand the shock load without failure. The following calculations were performed to determine the appropriate nominal diameter of the eye bolt, given that the shock load is reduced by a factor of 5 using the flexible shock cord. The allowable stress for the eye bolt was selected as 100 MPa to minimize its deformation. The eye bolts are made from stainless steel and coated with zinc to slow down corrosion.

#### Design Considerations:

- Load Reduction Factor: 0.7
- Shock load: 470 kg
- Allowable Stress allowed for the bolt:  $\sigma = 100 \text{ MPa}$
- Acceleration due to Gravity:  $g = 9.81 \text{ m/s}^2$

First, the load in kilograms was converted to Newtons then divided by the load reduction factor yielding a load of 3186.8 N:

The nominal bolt diameter was calculated using equation (3.7):

$$P = \frac{\pi}{4} d_c^2 \times \sigma \quad (3.7)$$

where:

- $P$  is the load in Newtons
- $\sigma$  is the allowable stress in pascals

Rearranging the equation and solving for  $d$ , the diameter of the eye bolt was obtained as 6.36 mm, the nearest dimension for the bolt was then selected as 8 mm.

The eye bolts were purchased and attached to each bulkhead in the configuration shown in figure 3.4.

### 3.1.7 Bulkhead Screws Design

Bulkhead screws are used to secure the avionics bay to the airframe and the number of screws used need to be selected based on the shear stress they exert on the airframe. The following calculations were performed to ensure the screws could handle the shear stresses as well as prevent damage to the airframe.

#### Design Considerations:

- Material: Stainless steel due to its high shear strength hence allows us to work with smaller diameter screws
- Shear Strength: 65% of UTS, where UTS = 505 MPa
- Selected Screw Diameter,  $d = 5$  mm
- Number of screws,  $n = 6$
- Shear Force:  $P_s = 3186.8$  N

Using The shear stress  $\tau$  was calculated using equation (3.8):

- $P_s = 3186.8 \text{ N}$  is the shear force
- $d = 5 \text{ mm}$  is the screw diameter
- $n = 6$  is the number of screws

Rearranging to solve for  $\tau$ ,the calculated shear stress was obtained as:

$$\tau = 27.05 \text{ MPa}$$

This shear stress value was compared with the material's shear strength(44.8MPa) to ensure it would not shear off.

## 3.2 Electrical Design

The electrical module in the dual recovery system is a critical component that enables control and power management of the system. It encompasses various electrical components, circuits and systems that facilitate the effective operation of the dual recovery system. The elctrical module includes a 7.4V, 5000mAh power supply consisting of 3.7V-18650 Lithium Ion cells.Below is a block diagram of the electrical subsystem.

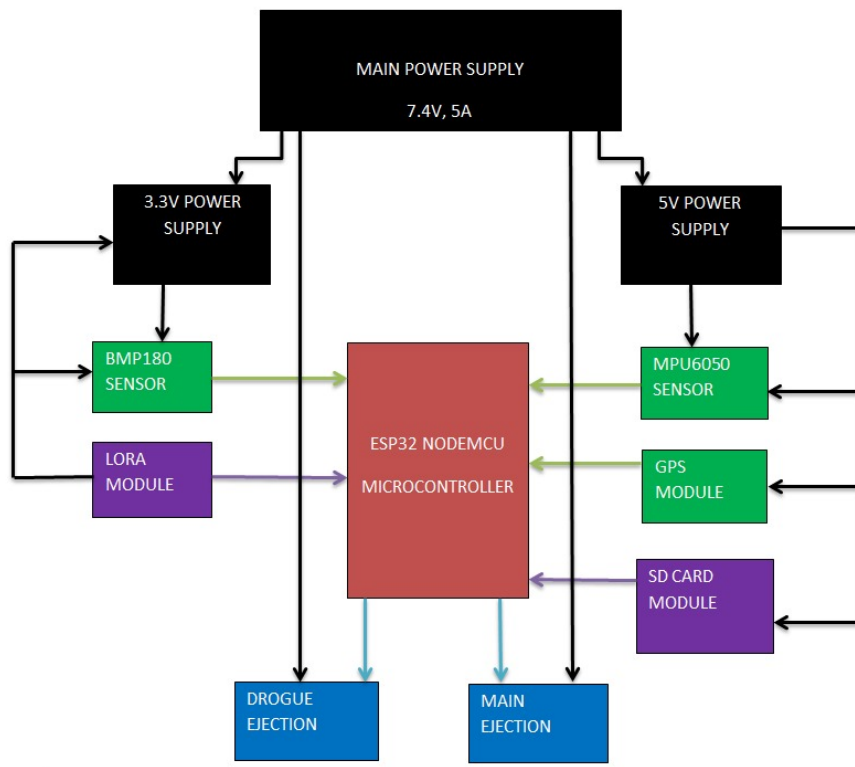


Figure 3.5: Dual recovery system electrical block diagram

The power supply system includes two buck converters, one to supply power to the components with a voltage rating of 3.3V and the other to power the electronic components rated 5V.

The ESP32-Nodemcu microcontroller acts as the brain of the electrical module. It receives altitude data from the BMP-180 sensor, acceleration and orientation data from the MPU-6050 sensor and location data from the GPS module. It then interprets this data to determine the state of flight of the rocket, igniting the ejection charge at the desired moments. The ejection charges are ignited by the glow of nichrome wire, powered by the 7.4V, 5000mAh supply.

### 3.2.1 Design considerations for the electrical module

The following considerations were observed when designing the electrical module for the proper functioning of the system

1. The design should generate enough power to run all the sensors, microcontroller and the charge igniters concurrently.
2. The ignition circuit should provide enough power to heat the nichrome wire within 4 seconds.
3. The flight computer board should be limited to dimensions not exceeding 200mm by 85mm.

### 3.2.2 Sensors

Three types of data are important for full recovery of the rocket, altitude, position and orientation , as well as location. To obtain these data, a BMP-180 sensor is used to determine altitude, the MPU-6050 is used to measure acceleration and orientation , and a NEO-6M GPS module provides location data.

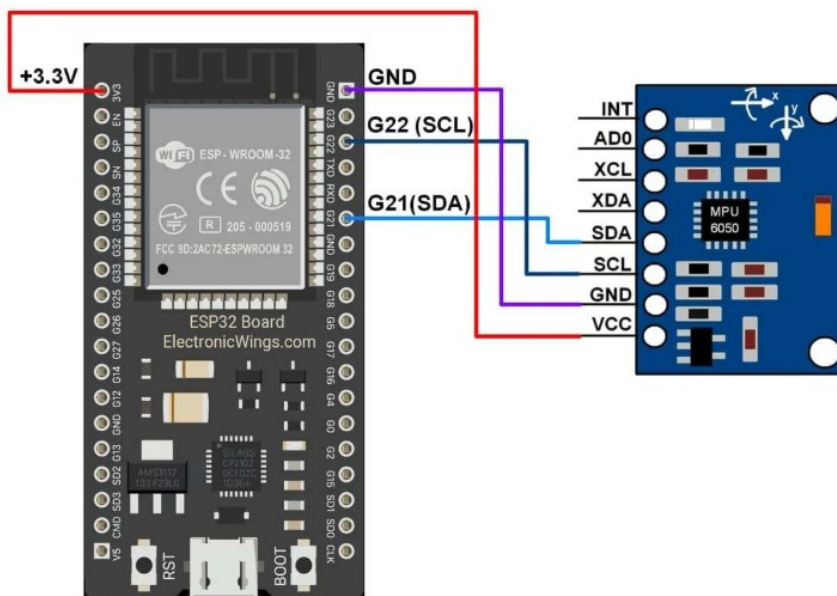


Figure 3.6: MPU-6050 sensor connection to ESP-32

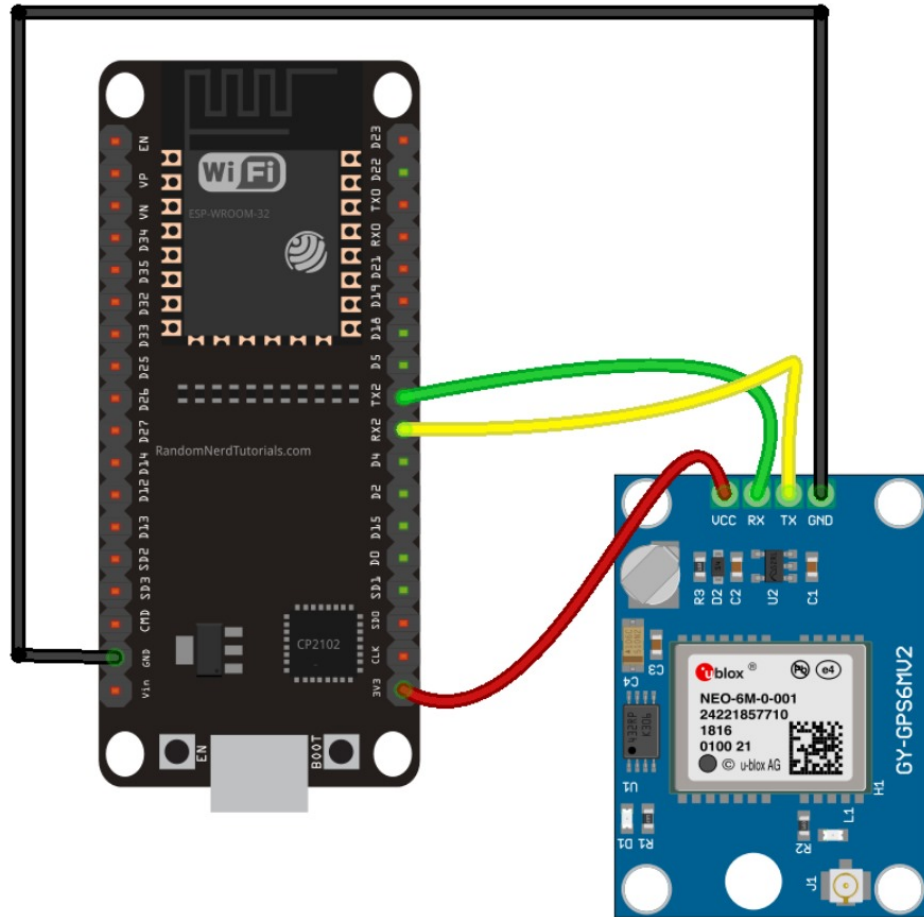


Figure 3.7: GPS sensor connection to ESP-32

The BMP-180 and the MPU-6050 sensors communicate with the microcontroller via Inter-Integrated circuit communication protocol, hence connected to the same pins on the esp32, that is, the serial clock pin and the serial data out pin, and distinguished by the microcontroller through their unique device addresses stored in the sensors' EEPROM.

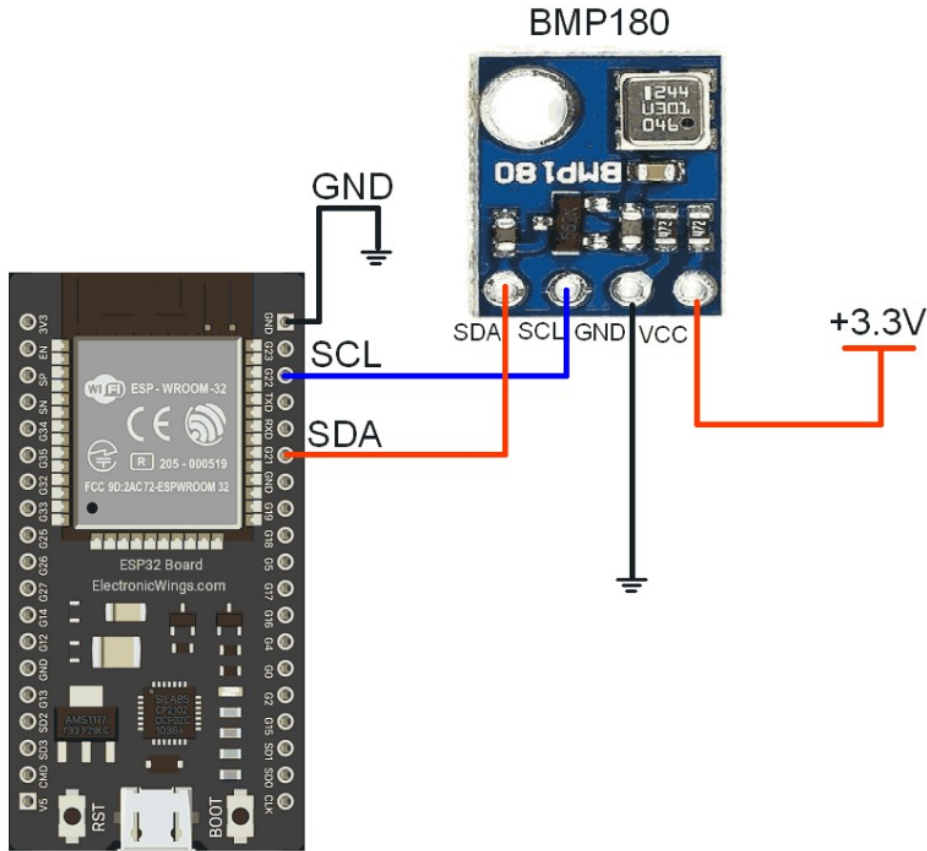


Figure 3.8: BMP-180 module connection to ESP-32

### 3.2.3 Telemetry

The SD card module communicates with the microcontroller using the SPI communication protocol. Once the sensors are initialized and start sending data, they are stored on an SD card in the SD card module.

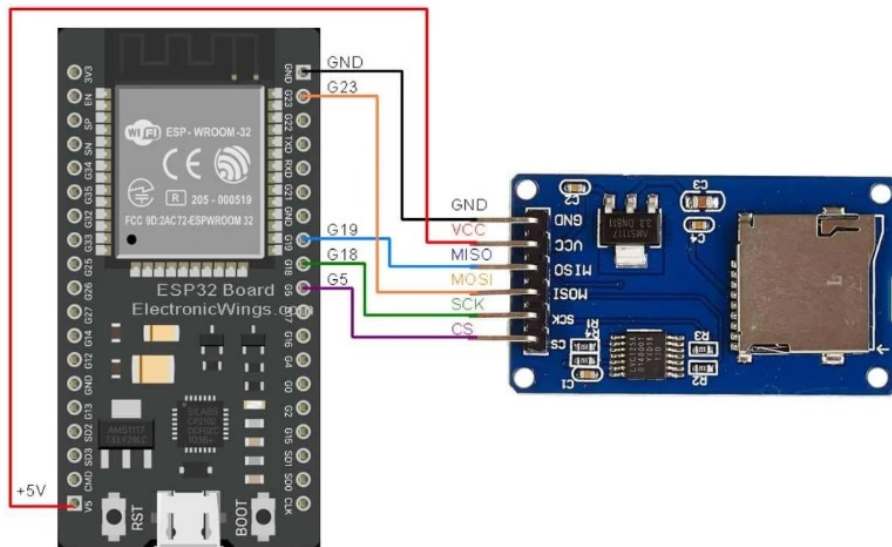


Figure 3.9: SD card module connection to ESP-32

To communicate with the base station, two methods were implemented, WiFi communication and Long Range wireless communication, also known as LoRa.

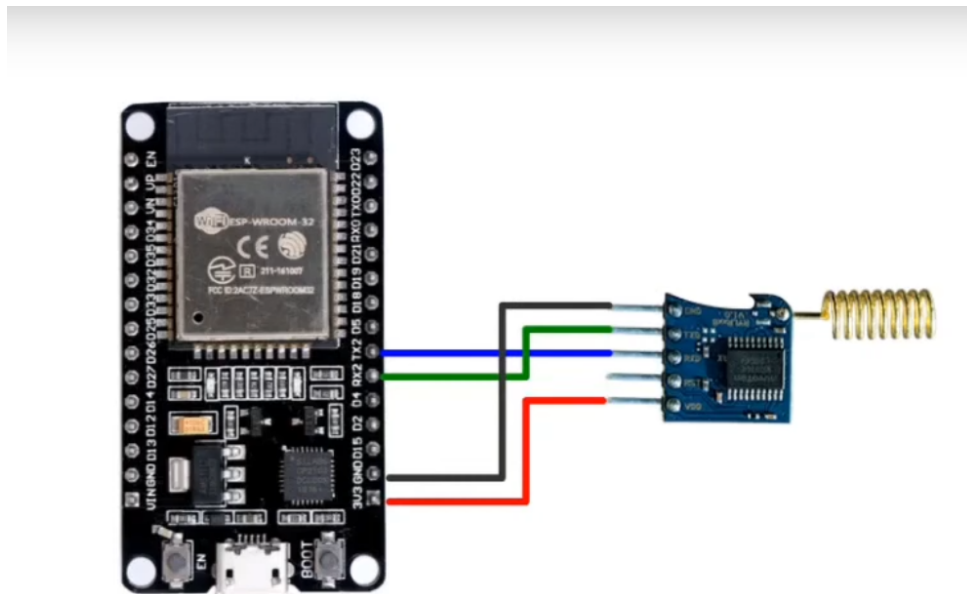


Figure 3.10: Lora module connection to ESP-32

### 3.2.4 Flight Computer Power Requirements

The following tables provides the power requirements for all the circuitry components used in the system, as well as the power calculations for each component. This includes both the operational and total power consumption across different voltage rails. The operation currents for each module was obtained from their respective datasheets.

Sensor	Voltage (V)	Current (A)	Power (W)
BMP180	3.3	0.000005	0.0000165
MPU6050	3.3	0.0039	0.01287
GPS NEO-6M	5.0	0.067	0.335

Table 3.2: Power Requirements for Sensors

Telemetry Component	Voltage (V)	Current (A)	Power (W)
LoRa RLYR890 UART Module	3.3	0.12	0.396
SD Card Module	3.3	0.1	0.33

Table 3.3: Power Requirements for Telemetry Components

The flight computer integrates two ignition circuits designed to ignite the ejection charges during flight. To determine the power consumed by these circuits, we developed a model to estimate the current flow through nichrome wire of varying lengths and resistances. In previous designs, the power supply system operated at 14.8V, delivering a current of 8A through the nichrome wire.

For this iteration, we aimed to achieve ignition using a lower voltage supply. To maintain the required 8A current, we utilized a shorter nichrome wire of length 35mm from the previous 90mm, thereby reducing its resistance. This adjustment ensured that the heat energy dissipated by the wire, governed by Joule's Law ( $Q = I^2Rt$ ), remained sufficient for ignition. Since heat energy depends quadratically on current, linearly on resistance, and proportionally on time, reducing the wire length allowed us to achieve the necessary thermal output within the same time frame, despite operating at a lower voltage.

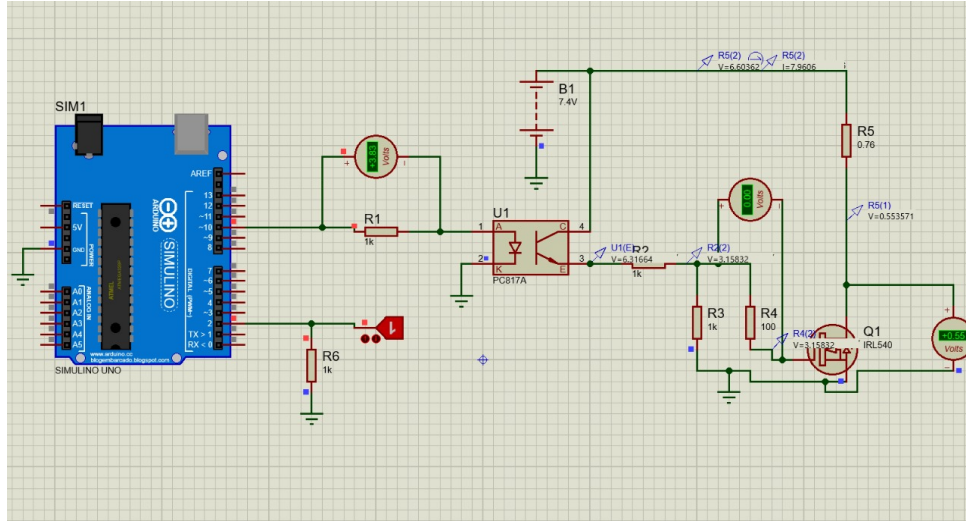


Figure 3.11: A model of the ignition circuit in Proteus

The power supply for this system consists of two 2500mAh lithium-ion cells arranged in series to provide a capacity of 7.4V and 5000mAh. Although the nominal continuous discharge rate of these cells is 1C, equating to 5A in this configuration, the ignition circuit successfully operates at 8A due to the cells' ability to handle higher peak currents. 18650 lithium-ion cells can momentarily provide discharge rates of up to 2C or more, enabling this configuration to meet the system's requirements. Furthermore, since the ignition circuit operates only for short bursts, the cells experience minimal thermal stress, ensuring their safety and reliability in this application.

Ejection System	Voltage (V)	Current (A)	Power (W)
Main Ignition Circuit	7.4	8.0	44.4
Drogue Ignition Circuit	7.4	8.0	44.4

Table 3.4: Power Requirements for Ejection System

### Power Requirement:

$$\text{Total Power (5V modules)} = 0.8 \text{ W} + 0.335 \text{ W} = 1.135 \text{ W} \quad (3.8)$$

$$\text{Total Power (3.3V modules)} = 0.0000165 \text{ W} + 0.01287 \text{ W} + 0.396 \text{ W} = 0.4088865 \text{ W} \quad (3.9)$$

$$\text{Ejection Circuit Power (Max)} = 7.4 \text{ V} \times 6 \text{ A} = 44.4 \text{ W} \quad (3.10)$$

$$\text{Total Power Requirement (Max)} = 1.135 \text{ W} + 0.4088865 \text{ W} + 44.4 \text{ W} \quad (3.11)$$

$$\text{Total Power Requirement (Max)} \approx 45.94 \text{ W} \quad (3.12)$$

The calculated maximum power requirement of 45.94W is based on the combined power consumption of all components, including the ejection circuits. However, the system is designed with a 2C-rated Li-ion battery, which provides a discharge rate of 2 times its capacity, equating to 10A for a 5000mAh battery. This discharge rate allows the system to handle short bursts of higher power demand, such as when the ejection circuits are activated. Despite the peak requirement of 44.4W from the ejection circuits alone, the battery can provide the necessary current without exceeding its rated discharge capacity. Therefore, although the maximum theoretical power requirement exceeds the battery's continuous output capacity, the battery's ability to provide short bursts of higher current ensures the system can operate safely within its design parameters, with an actual maximum sustainable power consumption of 37W.

**Fabrication of the electrical module** A flight computer schematic was developed as per the design requirements using EasyEDA standard version.

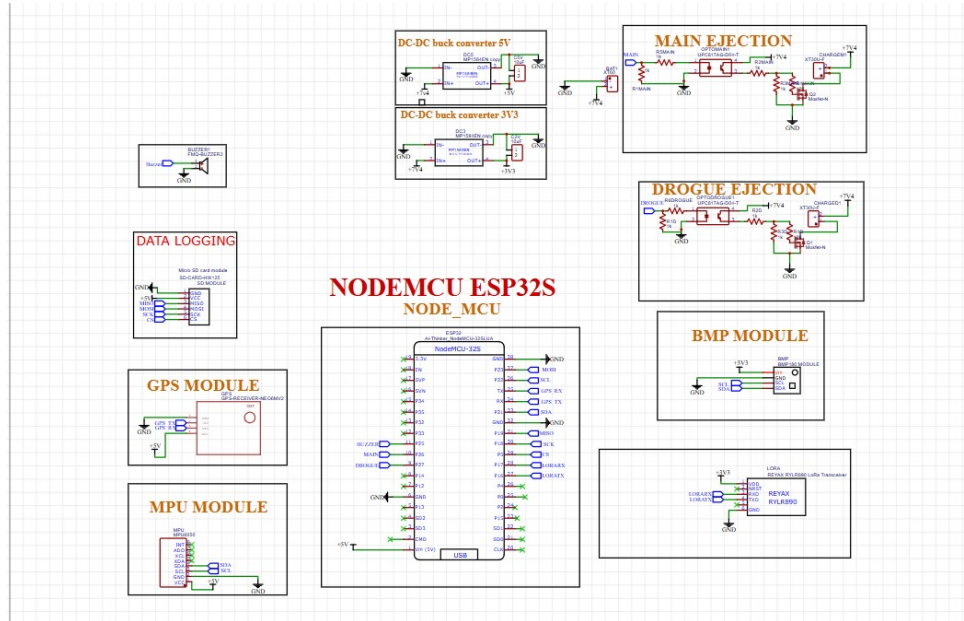


Figure 3.12: Flight computer schematic

Based on the schematic, a double layer copper clad of dimensions 77mm by 180 mm was cut on a guillotine machine. The patterns of tracks to be etched were printed on a glossy paper using a laser printer then transferred to the copper clad by ironing the paper containing the pattern against the corresponding face. One side of the pattern to be printed by the laser printer was mirrored so as to align with the corresponding pins on the other side of the copper clad. The copper clad with the pattern was then placed in a bowl containing a 1:1 mixture of Hydrochloric Acid and Hydrogen peroxide—which were the etching agents. Holes for soldering components as well as vias to connect the tracks on both sides of the board were drilled on a bench drill using a 1mm drill bit. The results were as shown in the diagrams below

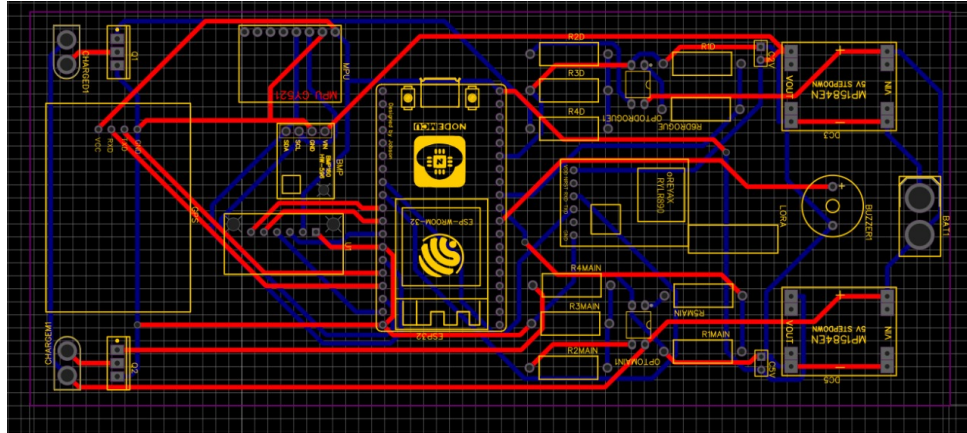


Figure 3.13: Flight computer PCB

### 3.2.5 Telemetry

The project required the transmission of sensor data upto 3km in altitude from an MPU6050, a GPS module, and a BMP sensor. To ensure effective communication, the data was organized into a structured format and transmitted at a frequency of 10 times per second.

The data structure was designed as follows:

- **MPU6050:** 6 axes of data (3 accelerometers + 3 gyroscopes) each at 2 bytes, totaling 12 bytes.
- **GPS Module:** Coordinates (latitude and longitude) at 4 bytes each, totaling 8 bytes.
- **BMP Sensor:** Temperature and pressure, each at 2 bytes, totaling 4 bytes.

Combining these, the total data payload per transmission was:

$$\text{Total Payload} = 12 \text{ bytes(MPU6050)} + 8 \text{ bytes(GPS)} + 4 \text{ bytes(BMP)} = 24 \text{ bytes}$$

Given that the data was to be transmitted 10 times per second, the required bandwidth was calculated as follows:

$$\text{Bandwidth} = \text{Total Payload} \times \text{Transmission Frequency}$$

$$\text{Bandwidth} = 24 \text{ bytes} \times 10 \text{ Hz} = 240 \text{ bytes/sec}$$

To convert this to bits per second:

$$\text{Bandwidth} = 240 \text{ bytes/sec} \times 8 \text{ bits/byte} = 1920 \text{ bits/sec or } 1.92 \text{ kbps}$$

LoRa offers bandwidths of up to 27 kbps, and since the required data rate is 1.92 kbps, LoRa satisfies the data transmission bandwidth requirement. Moreover, LoRa offers a line of sight range of 15-20km therefore LoRa satisfies the transmission range requirement to be selected as the communication module for the task.

### 3.3 Software Design

The software and control module is a crucial component that determines the different stages of flight for the rocket. It ensures precise timing for deploying the main and drogue parachutes while also prioritizing user-friendliness for base station operators.

#### 3.3.1 Design Considerations

The software and control module was designed with the following considerations:

1. The module should accept flight data from the flight computer sensors.
2. Implement data processing to detect different flight stages using sensor inputs.
3. Define and use predefined thresholds and flight stages to determine specific conditions for flight stage transitions (State Machine).
4. Utilize a Kalman Filter Algorithm for accurate and real-time data processing, accounting for potential noise and discrepancies in sensor data.
5. Make precise decisions on parachute deployment based on detected flight states by sending signals to trigger the deployment mechanism at the correct time.
6. Design a user interface for ease of operation by ground station personnel, providing clear visual feedback on system status.

### 3.3.2 Kalman Filter Algorithm

The Kalman filter algorithm processes altitude readings from the BMP180 sensor to reduce noise and provide a more accurate estimate of altitude. It achieves this by combining two pieces of information:

- **Predicted Altitude:** The filter predicts the next altitude based on the current estimate and a known variance in the system (process variance).
- **Measured Altitude:** It then compares this prediction with the actual altitude measured by the BMP180 sensor and calculates the weighting between the measured and predicted values using a "Kalman Gain."

#### Steps of the Algorithm:

1. Predict the next altitude and its uncertainty.
2. Compare the prediction to the sensor's measurement.
3. Adjust the altitude estimate by combining the prediction and the measurement.
4. Update the uncertainty based on this adjustment.

This approach smooths out noise from the sensor, resulting in a more accurate and stable altitude reading.

**2D Kalman Filter:** The 2D Kalman filter extends this concept to estimate two variables simultaneously: altitude and vertical velocity. It uses data from the BMP180 (altitude) and MPU6050 (motion/acceleration). This is especially useful for dynamic systems like the N4 rocket, where both position and speed must be monitored. By combining multiple sensor inputs, the filter provides accurate estimates of how high and fast the rocket is moving, even with noisy sensor data.

### 3.3.3 State Machine

The state machine defines and manages the rocket's flight phases. It comprises two key components:

- **States:** Represent the current system status.
- **Transitions:** Rules or conditions dictating when the system moves from one state to another.

#### States and Transitions:

##### 1. PREFLIGHT:

- **Description:** The system is in standby, waiting for the rocket to launch.
- **Transition Conditions:**
  - Acceleration (AccYInertial) exceeds 0.3 m/s<sup>2</sup>.
- **Next State:** POWERED\_FLIGHT.

##### 2. POWERED\_FLIGHT:

- **Description:** The rocket is actively ascending under powered thrust.
- **Transition Conditions:** Transition to APOGEE occurs when at least two out of three conditions are met:
  - The rocket's roll increases beyond 60 degrees
  - Vertical velocity (VelocityVerticalKalman) is less than 1.
  - The rocket's yaw increases beyond 60 degrees
- **Next State:** APOGEE.

##### 3. APOGEE:

- **Description:** The rocket reaches its highest altitude.

- **Actions:** Deploys drogue parachute.
- **Transition Conditions:** Altitude starts decreasing.
- **Next State:** DROGUE\_DESCENT.

#### 4. DROGUE\_DESCENT:

- **Description:** The rocket descends under the drogue parachute.
- **Transition Conditions:** Altitude drops below a predefined threshold for main parachute deployment.
- **Next State:** MAIN\_DESCENT.

#### 5. MAIN\_DESCENT:

- **Description:** The main parachute is deployed for a controlled descent.
- **Transition Conditions:** Altitude reaches a ground proximity threshold (e.g., 10 meters above ground level).
- **Next State:** POSTFLIGHT.

#### 6. POSTFLIGHT:

- **Description:** The rocket has landed and system operations cease.
- **Actions:** Disable sensors and log final data.

#### 3.3.4 Variables

- **flightState:** Stores an integer representation of the current state for potential external use (e.g., telemetry).
- **AltitudeKalman:** The estimated altitude of the rocket.
- **AccYInertial:** The rocket's acceleration in the vertical direction.
- **VelocityVerticalKalman:** The rocket's vertical velocity.

**Code Implementation:** The implementation uses the following key elements:

- **Enum for States:** The enum `State` defines all the possible states in the system.  
`State currentState = PREFLIGHT;` sets the starting state.
- **Switch-Case Logic:** Each case corresponds to a state (PREFLIGHT, POWERED\_FLIGHT, etc.). Inside each case, the code checks conditions for transitioning to the next state.
- **Conditions:** The `if` statements inside each case determine whether to transition to a new state based on sensor data.
- **Looping:** The `while (true)` loop keeps checking the conditions continuously, ensuring the system always responds to real-time data.

This design ensures iterative state checking and accurate transitions when predefined conditions are satisfied.

### 3.3.5 User Interface

The User Interface is a web-based application titled **Nakuja N4 Rocket Dashboard**. The dashboard is designed to provide real-time telemetry data and status updates for the N4 rocket. The layout is user-friendly, with an emphasis on critical flight parameters and visual clarity. A dark theme with contrasting colored text and icons is used to ensure readability and reduce eye strain in various lighting conditions. The branding also reflects the branding of the project while maintaining professional formatting.

#### Design considerations for the User Interface.

- The UI values should be dynamically linked with sensor feeds using MQQT protocol to provide live telemetry during the rocket's operation.
- Data arranged logically, with flight dynamics on the top row and geospatial/temporal data on the bottom row for easier monitoring.

- Modular layout that is adaptable to various screen sizes.
- Incorporated color changes in labels or data boxes to visually indicate threshold conditions.

## Components of the Dashboard.

### 1. Apogee Thresholds Panel

**Purpose:** Monitors critical conditions that indicate apogee (the highest point of the rocket's flight path).

#### Indicators:

- **Acceleration:** Displays "Awaiting" to indicate acceleration threshold has not been met yet.
- **Yaw > 60:** Indicates the lateral deviation threshold of 60 degrees for apogee detection.
- **Roll > 60:** Tracks roll angles greater than 60 degrees, which is the third threshold for apogee detection.

#### Rocket Status:

- A colored labeled button shows the rocket's current operational state. This is likely dynamic and will change as the rocket transitions through its flight phases.

### 2. Real-Time Telemetry Panels

These panels display real-time telemetry data relevant to the rocket's performance and flight conditions. Each metric is highlighted in a dedicated box with an associated icon for quick visual identification:

- **Altitude (Center Top-Left):** Measured in meters (m). Indicates the rocket's vertical distance from the ground.

- **Velocity (Center Top-Middle):** Measured in meters per second (m/s). Represents the rocket's speed.
- **Acceleration (Center Top-Right):** Measured in meters per second squared ( $\text{m/s}^2$ ). Displays the rate of change of velocity.
- **Latitude (Center Bottom-Left):** Provides the rocket's current latitude coordinates.
- **Longitude (Center Bottom-Middle):** Displays the rocket's longitudinal position.
- **Time (Center Bottom-Right):** Represents the flight time since launch.

**Iconography.** Each data box includes an icon that visually represents the metric:

- **Altitude:** A stacked disk representing layers of height.
- **Velocity:** A forward-pointing arrow for motion.
- **Acceleration:** Circular lines representing rotational forces or momentum.
- **Latitude/Longitude:** Globes with location markers for geospatial data.
- **Time:** A refresh or timer icon to emphasize its dynamic nature.

## 4 Results and Discussion

### 4.1 Main and Drogue Parachute

The drogue and the main parachutes were modeled using Solidworks CAD software. Design calculations for hemispherical parachutes was referenced from FreeCAD software. The design calculations indicated that a canopy area of approximately  $0.471 \text{ m}^2$  was required to achieve the desired terminal velocity of  $21 \text{ m/s}$ . The calculated diameter of the parachute canopy was  $77.4 \text{ cm}$ , with a corresponding circumference of  $2.43 \text{ m}$ . The chosen number of gores was 8, and the spill hole area was  $0.047 \text{ m}^2$ . These parameters ensured that the drogue parachute effectively slowed the rocket and stabilized it before the deployment of the main parachute.

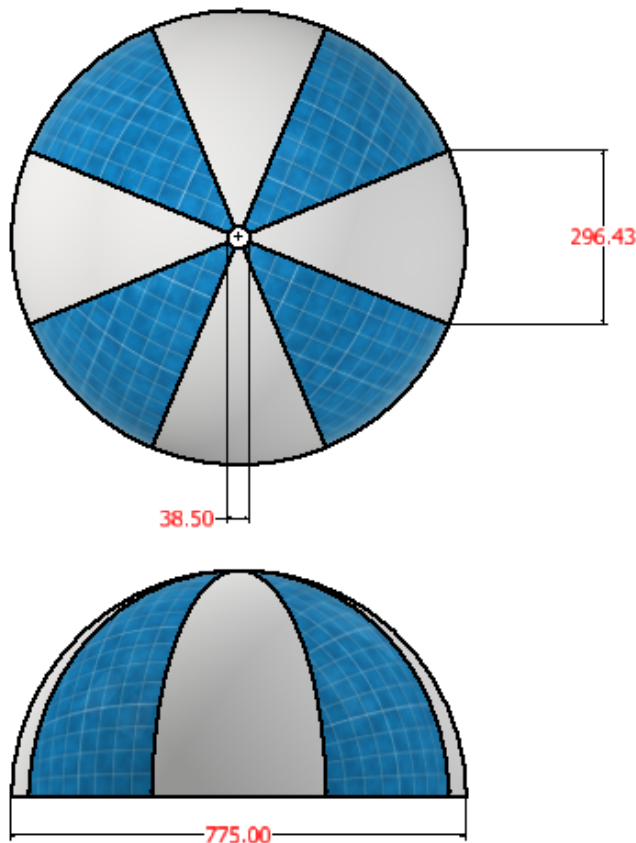


Figure 4.1: Assembly drawing of the drogue parachute



Figure 4.2: Fabricated drogue parachute

For the main parachute, the required canopy area was determined to be  $6.869\text{ m}^2$  to achieve a terminal velocity of  $5.5\text{ m/s}$ . The diameter of the main canopy was calculated to be  $2.957\text{ m}$  with a circumference of  $9.293\text{ m}$ . The parachute design included 20 gores, and the spill hole area was  $0.069\text{ m}^2$ . These specifications aimed at ensuring a soft and controlled landing by significantly reducing the rocket's descent speed.

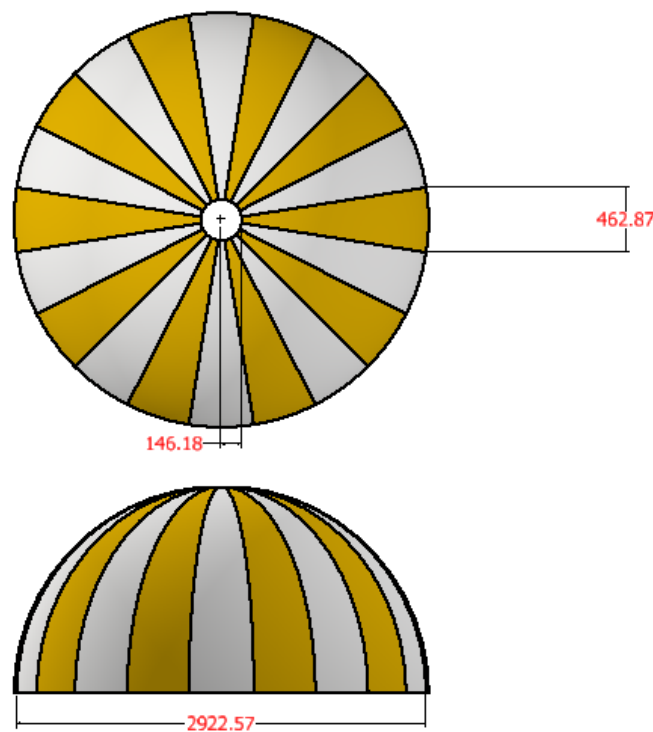


Figure 4.3: main chute



Figure 4.4: Fabricated main parachute

## 4.2 Avionics Bay

The avionics bay was also modeled using the Solidworks CAD package. The CAD model , assembly file with dimensions the finished part are provided. All the part designs are included in the appendix. Figure 4.5 and 4.6 shows the mechanical design of the avionics bay with its respective overall dimensions.

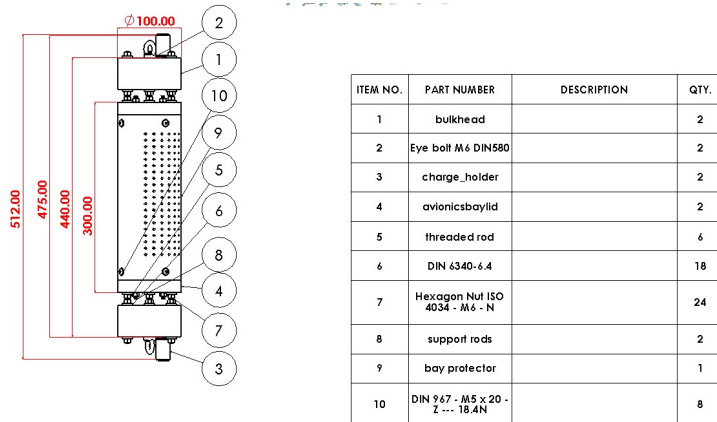


Figure 4.5: 3D model of the avionics bay

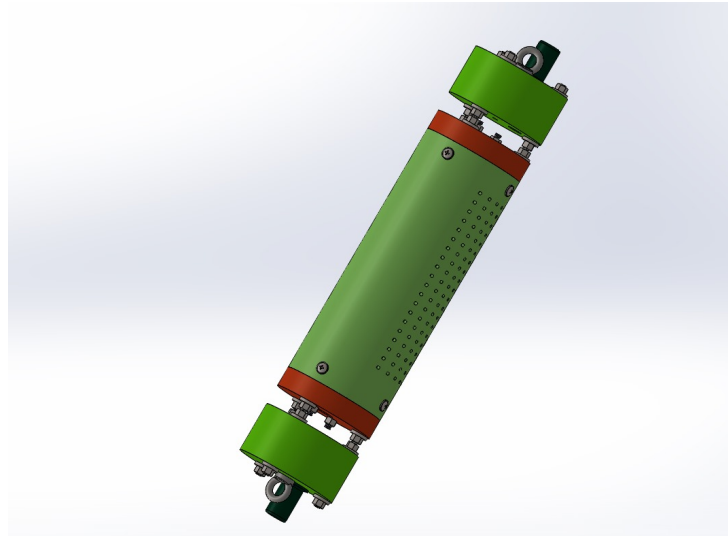


Figure 4.6: avionics bay model

Figure 4.7 shows the fabricated avionics bay. The bay fits perfectly within the rocket's airframe and the flight computer fits well within the avionics bay housing. The entire weight of the system has been measured to be 2157 grams, which is less than a third of the total assigned weight threshold for the recovery system ,set as 6 kg by the N4 rocket airframe team.

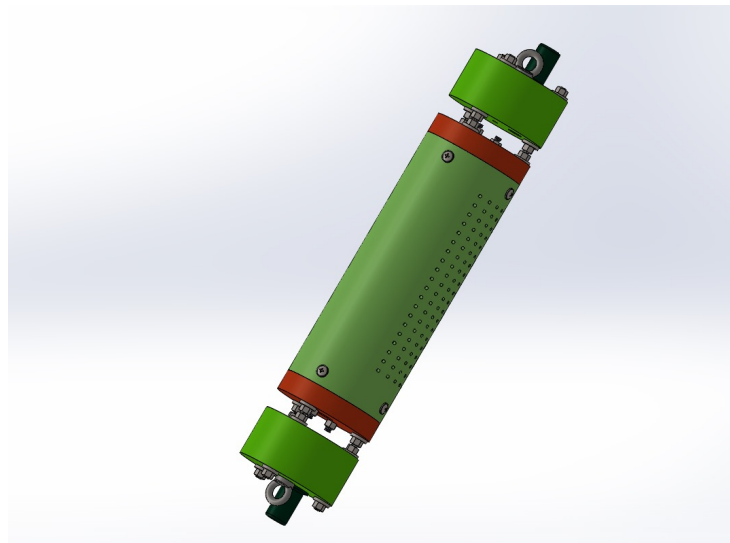


Figure 4.7: Fabricated avionics bay

Table 4.1: Shock Cord Material Selection

Section	Material	Purpose
Lower (50mm)	Kevlar	To protect the tubular nylon cord from high temperatures of ejection charge
Upper (8000mm)	Tubular Nylon	To absorb the opening shock from destroying the canopy

Table 4.2: Selection of shock cord width

Thickness	Width	Breaking Weight
0.08" (2.032mm)	5/8" (15.875mm)	1500lbs (680kg)
	1.25" (31.75mm)	3200lbs (1450kg)

### 4.3 Eye Bolt

The eye bolt was designed to handle significant loads, with a calculated diameter of approximately 6.36 mm. Considering practical availability, an 8 mm diameter was selected.

This eye bolt was essential for securely attaching the shock cords and needed to endure the shock loads during deployment. The load reduction factor used ensured that the bolt remained within safe operational limits under expected forces.

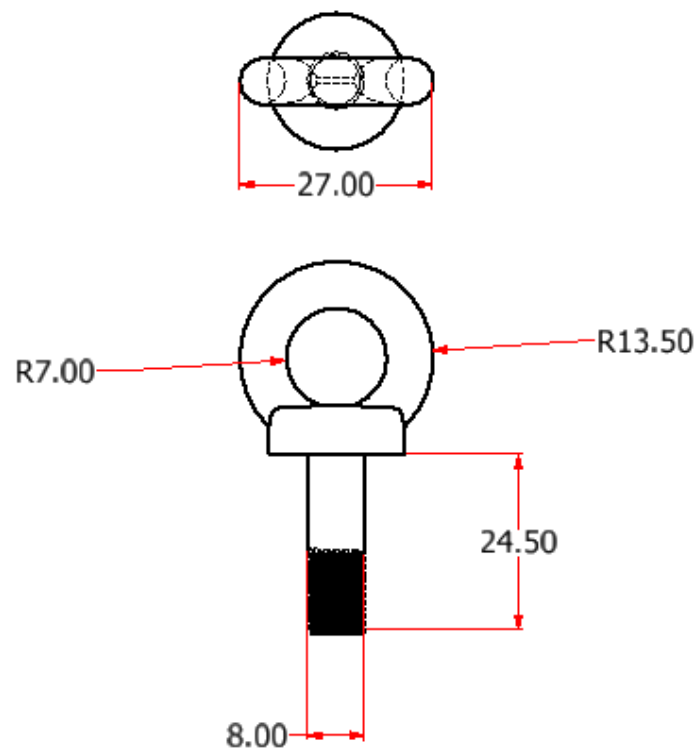
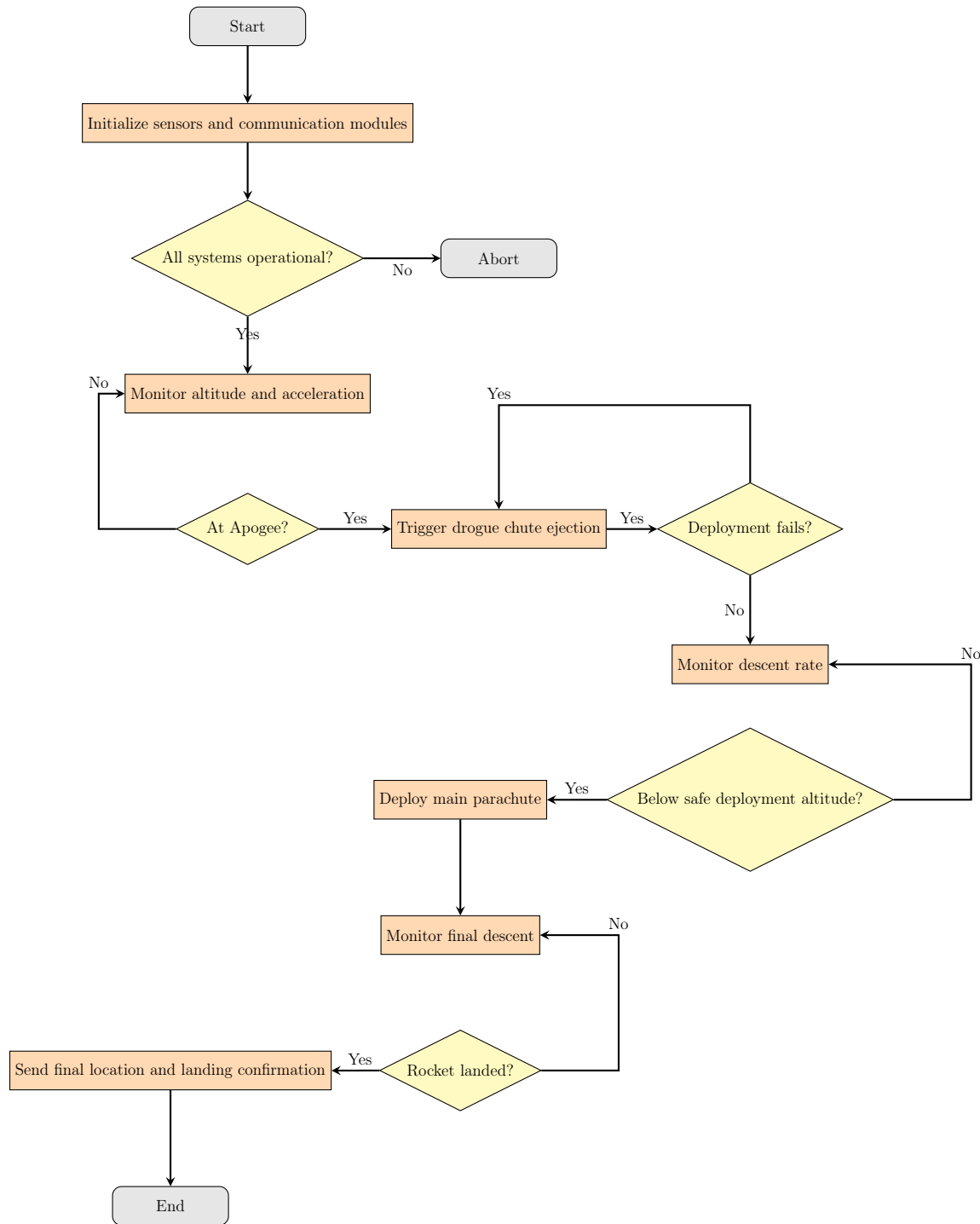


Figure 4.8: drogue chute

## 4.4 Control Flowchart



The dual recovery system for a high-speed powered rocket begins by initiating the sensors and communication module to monitor the rocket's status. It then checks if all systems are operational; if not, the process is aborted. If the systems are functioning

properly, the rocket's altitude and acceleration are monitored. Upon reaching apogee, the highest point in its flight, the drogue chute is deployed to slow the rocket's descent. The system checks whether the deployment was successful. If the drogue chute fails to deploy, the system monitors the descent, otherwise, it continues to check the descent rate. As the rocket descends, the system determines if it has dropped below a safe altitude for deploying the main parachute. If the altitude is safe, the main parachute is deployed to slow the rocket further for final descent. Throughout the descent, the system checks for a safe landing. Once the rocket lands, the system sends the final location and landing confirmation, marking the end of the process.

## 4.5 Control and Software Module

The control and software module accepts input from the flight computer sensors. The table 4.3 lists the input data provided by the sensors to the software and control module.

The control module processes flight data using a Kalman filter algorithm to smooth out fluctuations in the raw sensor data, providing more reliable estimates of key metrics. The inputs to the Kalman filter include:

- **Altitude (bmpAltitude):** Measurement from the BMP180 sensor.
- **Vertical Acceleration (AccZInertial):** Measurement from the MPU-6050 accelerometer.

The Kalman filter outputs refined metrics, improving the accuracy of altitude and movement estimation.

The state machine of the control module receives the following key metrics to determine flight state transitions:

- **Altitude (Altitude Kalman):** Filtered altitude measurement from the BMP180 sensor.

Table 4.3: Measured Metrics

Metric	Source	Metric Units
Acceleration (X-axis)	MPU-6050 accelerometer	m/s <sup>2</sup>
Acceleration (Y-axis)	MPU-6050 accelerometer	m/s <sup>2</sup>
Acceleration (Z-axis)	MPU-6050 accelerometer	m/s <sup>2</sup>
Angular Velocity (Pitch)	MPU-6050 gyroscope	°/s
Angular Velocity (Roll)	MPU-6050 gyroscope	°/s
Angular Velocity (Yaw)	MPU-6050 gyroscope	°/s
Temperature	BMP180 sensor	°C
Pressure	BMP180 sensor	Pa
Latitude	NEO-6M GPS module	degrees
Longitude	NEO-6M GPS module	degrees
Time (GPS)	NEO-6M GPS module	hh:mm:ss

- **Vertical Velocity (VelocityVerticalKalman):** Derived from MPU-6050 accelerometer data and altitude measurements.
- **Inertial Acceleration (AccYInertial):** Adjusted for tilt using pitch and roll angles.
- **Pitch Angle (AnglePitch):** Orientation relative to the ground, calculated from accelerometer data.

These metrics are used to monitor state transitions such as PREFLIGHT, POWERED\_FLIGHT, COASTING, APOGEE, DROGUE\_DESCENT, MAIN\_DESCENT, and POSTFLIGHT.

The control module communicates key data metrics to the User Interface via the MQTT protocol for real-time updates on the base station dashboard. An example of a payload sent by the control module is shown below:

```
{
  "flightstate": 2,
  "acceleration": 0.85,
  "yaw": 45.0,
  "roll": 59.0,
  "vertical_velocity": 19.3,
  "altitude": 0.3
}
```

The `flightstate` parameter corresponds to the current phase of the rocket's flight, as defined by the following mapping:

```
const statusMapping = {
  0: "Preflight",
  1: "Powered Flight",
  2: "Apogee",
  3: "Drogue descent",
  4: "Main descent",
  5: "Postflight"
};
```

## 4.6 User Interface

The Nakuja N4 Rocket Dashboard (see Fig. 4.9) is designed with a focus on clarity and usability. The dashboard features a dark theme for optimal visibility in various lighting conditions and a layout that prioritizes critical information. Its key components include:

- **Main Metrics Panel:** Displays real-time telemetry data such as:
  - Altitude: Current height above sea level.
  - Velocity: Vertical speed.

- Acceleration: Adjusted inertial acceleration.
- Latitude and Longitude: Rocket's geolocation.
- Time: Timestamp of telemetry data.



Figure 4.9: User Interface Main Dashboard Panel

- **Apogee Thresholds Panel:** Indicates Apogee detection through achievement of critical flight milestones (see Fig. 4.10).
- **System State Indicator:** Displays the current flight state using a dynamically updated button.

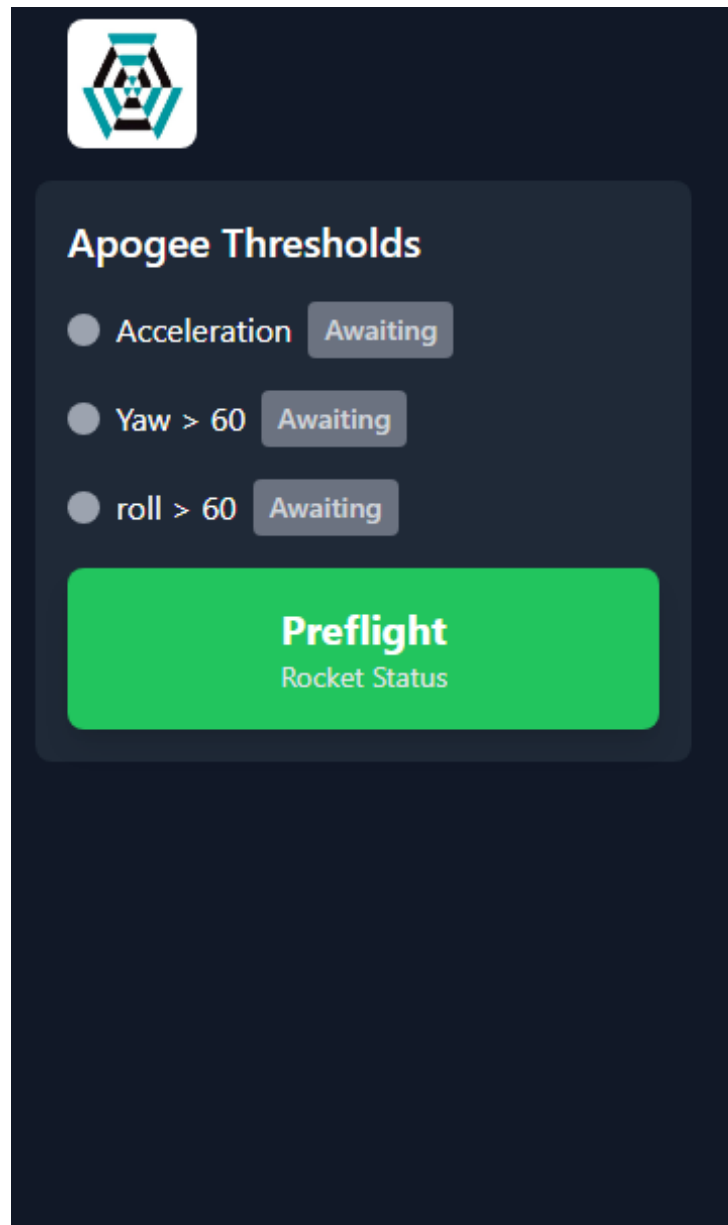


Figure 4.10: Apogee threshold panel

The User Interface is fully responsive, ensuring optimal usability across a range of devices, from small mobile screens (see Fig. 4.11) to large desktop monitors.

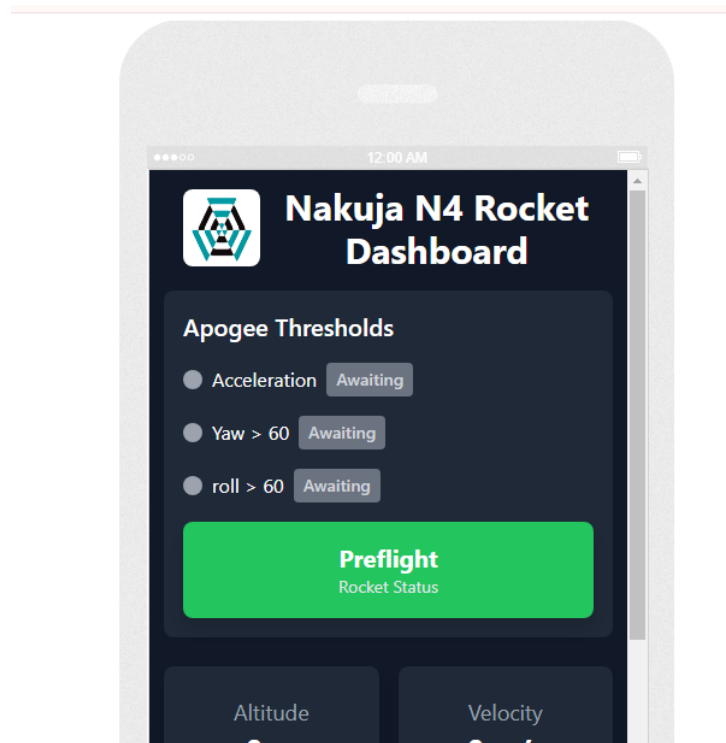


Figure 4.11: User Interface mobile view

## 5 Summary, Conclusion, and Future Work

The first phase of this project focused on designing a dual recovery ejection mechanism for the N4 high-power rocket, incorporating a 3D-printed avionics bay and machined bulkheads. The avionics bay, designed to house the control electronics, is powered by a 14.8V battery. MOSFET transistors are employed to activate the igniters at precise moments, while voltage regulation for the sensors and microprocessor is managed by buck converters. The ejection mechanism is controlled by a state machine algorithm, with sensor data filtered using a Kalman filter.

The recovery system utilizes nylon shear pins for controlled separation and a hemispherical drogue and main parachute for reliable performance and ease of fabrication. An electronic switch is included to arm the ejection mechanism, ensuring safety during handling.

With the design now complete, the next steps involve fabricating the components based on the finalized specifications. This includes 3D printing the avionics bay and coupler, machining the bulkhead, fabricating the parachutes, developing the electronic circuitry and code, and assembling the system.

## References

- [1] R. James, *Aerodynamics of Recovery Systems*. New York, NY: Aerospace Press, 1999.
- [2] J. Smith, “Advances in altimeter technology for high-power rocketry,” *Journal of Rocketry Technology*, vol. 7, pp. 120–135, 2019.
- [3] M. Williams, “Electronics advances in high-power rocketry,” *International Journal of Aerospace Engineering*, vol. 10, pp. 98–107, 2005.
- [4] R. Pearson, *Parachute Design and Engineering*. Los Angeles, CA: Skyrocket Publications, 2008.
- [5] S. Miller, “Modern innovations in rocketry,” *Journal of Advanced Rocketry*, vol. 5, pp. 50–70, 2023.
- [6] Tripoli Rocketry Association, “History of the tripoli rocketry association,” *Tripoli Rocketry Association Journal*, vol. 3, pp. 15–25, 2021.
- [7] J. Smith, “Advances in altimeter technology for high-power rocketry,” *Journal of Rocketry Technology*, vol. 7, pp. 120–135, 2019.
- [8] M. Williams, “Electronics advances in high-power rocketry,” *International Journal of Aerospace Engineering*, vol. 10, pp. 98–107, 2005.
- [9] E. Johnson, “Integration of gps technology in modern rocketry,” *Journal of Rocketry and Space Science*, vol. 12, pp. 200–215, 2020.
- [10] S. Miller, “Modern innovations in rocketry,” *Journal of Advanced Rocketry*, vol. 5, pp. 50–70, 2023.
- [11] P. Brown, “Signal processing in bps space dual recovery systems,” *Journal of High-Power Rocketry*, vol. 8, pp. 110–125, 2021.
- [12] M. Green, “Avionics systems in tra high-power rockets,” *Journal of Rocketry Technology*, vol. 6, pp. 80–95, 2019.

- [13] R. James, *Aerodynamics of Recovery Systems*. New York, NY: Aerospace Press, 1999.
- [14] R. Pearson, *Parachute Design and Engineering*. Los Angeles, CA: Skyrocket Publications, 2008.
- [15] T. Venner, “Material selection for parachute fabrication,” *Journal of Materials Science in Aerospace*, vol. 2, pp. 45–59, 1993.
- [16] A. Knight, “Pyrotechnic charges in aerospace applications,” *Aerospace Engineering Journal*, vol. 19, pp. 160–175, 1983.
- [17] FreeCAD, “Rocket ejection charge calculator,” 2021, accessed: 2024-08-20. [Online]. Available: [https://wiki.freecad.org/Rocket\\_Ejection\\_Charge\\_Calculator](https://wiki.freecad.org/Rocket_Ejection_Charge_Calculator)
- [18] W. Davis, “Mechanical ejection systems in model rocketry,” *Journal of Mechanical Engineering*, vol. 15, pp. 200–220, 2004.
- [19] D. Smith, “Enhancing safety in rocket parachute systems,” *Journal of Space Safety*, vol. 29, no. 3, pp. 111–125, 2022. [Online]. Available: <https://doi.org/10.1016/j.spacesafety.2022.04.002>
- [20] J. Anderson, “High-precision apogee detection algorithms for rocketry,” *Journal of Aerospace Engineering*, vol. 55, no. 4, pp. 789–803, 2021. [Online]. Available: <https://doi.org/10.1016/j.aerospace.2021.01.003>
- [21] E. Johnson, “Telemetry and data logging for high-power rocketeers,” *Space Technology*, vol. 48, no. 1, pp. 234–245, 2020. [Online]. Available: <https://doi.org/10.1016/j.spacetech.2020.07.001>
- [22] L. Miller, “Control systems for rocket parachute deployments,” *International Journal of Rocket Science*, vol. 33, no. 2, pp. 102–115, 2019. [Online]. Available: <https://doi.org/10.1016/j.ijrs.2019.05.007>

- [23] T. R. Association, “Advanced flight software and deployment systems,” Tripoli Rocketry Association, Tech. Rep., 2021. [Online]. Available: <https://www.tripoli.org/resources/flight-software-report-2021>
- [24] B. Douglas, *Kalman Filter Tutorial*. Resourcium, 2016. [Online]. Available: <https://resourcium.org/journey/introduction-kalman-filter>
- [25] P. Lab, “Kalman filter and testing | insight devlog 02,” *Phil’s Lab*, 2019. [Online]. Available: <https://phillabs.medium.com/kalman-filter-and-testing-insight-devlog-02-e7a2cba9ef70>
- [26] B. Space, “Telemetry system for high-power rockets,” 2021, available at: <https://bps.space/telemetry>.
- [27] Bzarg, “How a kalman filter works, in pictures,” *Bzarg*, 2013. [Online]. Available: <https://www.bzarg.com/p/how-a-kalman-filter-works-in-pictures/>
- [28] T. R. Association, “Telemetry and data communication in high-power rocketry,” 2020, available at: <https://www.tripoli.org/telemetry>.

# A Appendix

## A.1 Time plan

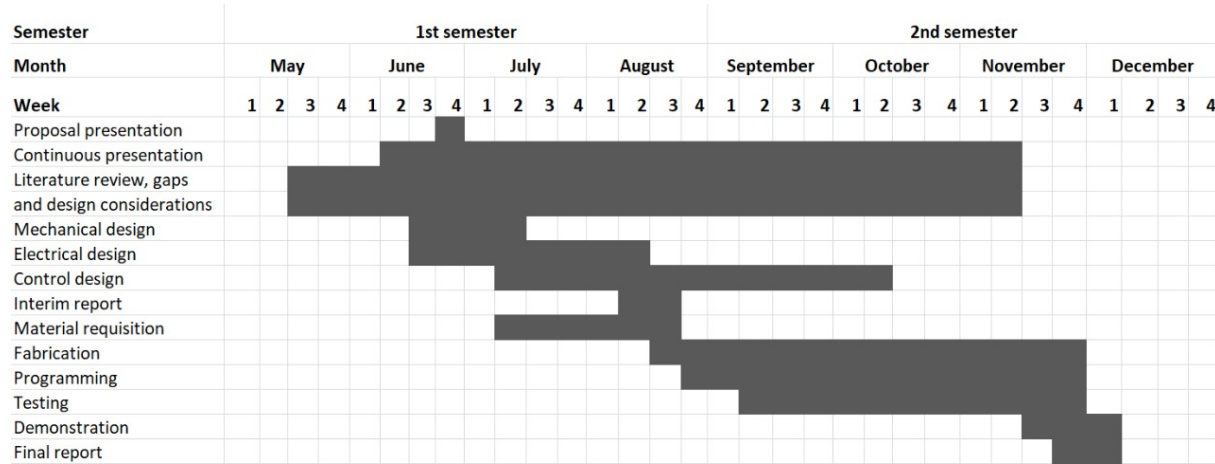


Figure A.1: Time plan

## A.2 Budget

No	Item	Description	Quantity	Cost per Unit (KES)	Total Cost (KES)
1	Filament	PLA	1	3,500	3,500
2	Drill Bits	Size M1, M2, M3	5	550	2,750
3	SD Memory Card Holder	San D Isk SD	1	300	300
4	USB Cable	Type B Micro	1	300	300
5	Wet Wipes	Travel Pack 40S	1	160	160
6	Lora Modules	Reyax RLR896	2	4,100	8,200
7	Gyroscope Sensor	MPU 6050	1	600	600
8	GPS Module	Neo-6M GPS module	1	400	400
9	MOSFET Transistor	N-channel IRL 540N	1	300	300
10	Resistors	100 and 1K ohms	10	50	500
11	Microcontroller	ESP32	1	1,800	1,800
12	Soft Nylon	100mm	1	1,725	1,725
13	Threaded Rods	6mm	1	450	450
14	Eye Bolts	10mm	2	480	960
<b>Total</b>					<b>21,945</b>

Table A.1: Budget for Items

### A.3 Production Plan

Week	Tasks/Activities	Material Required	Special Equipment	Sequential/Parallel Activities	Status/Remarks
1	Review of the previous semester's work with our supervisor	N/A	N/A	N/A	Done
2	Redesign the shock cord using the Pfanz method	N/A	N/A	N/A	Done
3	Mapping the project requirements and designing the user interface	N/A	N/A	Sourcing for electronic components required for the project	Done
4	Redesigning the power distribution board	N/A	N/A	N/A	Done
5	i. Making corrections to the interim report ii. Submission of the report	N/A	N/A	Improving the power distribution board design	Done
6	i. Fabrication of the avionics bay lids ii. Fabrication of the charge cartridges	PLA Filament	3D Printer	Redesigning the flight computer holder	Done
7	i. Etching the power distribution board PCB ii. Soldering components for the PDB onto the PCB iii. Testing the PCB	i. Copper clad ii. Hydrochloric acid iii. Hydrogen peroxide	i. Vertical drilling machine ii. Soldering station iii. Iron box	Interface the BMP180 sensor with the ESP32 microcontroller	Done
8	i. Etching the flight computer PCB ii. Soldering connector pins for the flight computer components onto the PCB iii. Connecting the flight computer to the power distribution board	i. Copper clad ii. Hydrochloric acid iii. Hydrogen peroxide	i. Vertical drilling machine ii. Soldering station iii. Iron box	i. Interfacing the MPU6050 with ESP32 microcontroller ii. Developing the filtering algorithm iii. Interfacing the LORA module with ESP32 microcontroller iv. Preparing the black powder	Done
9	i. Machining bulkheads ii. 3D printing avionics bay lid iii. 3D printing avionics bay protector iv. 3D printing flight computer holder	i. Soft Nylon rod ii. PLA filament	i. Centre lathe ii. 3D Printer	i. Interface the GPS module with the ESP32 ii. Developing the state machine algorithm iii. Implementing data logging iv. Conducting the first pop test v. Purchasing parachute fabrication material	Done
10	i. Cutting and stitching drogue and main parachutes ii. Stitching shroud lines	i. Ripstop Nylon ii. Nylon	Sewing machine	i. Developing the system web App and user interface ii. Conducting the second pop test	Done
11	Integration of the recovery system into the N4 rocket	N/A	Power drill	i. Implementing data logging ii. Carrying out the Drone test	Done
12	Rocket assembly dry run	N/A	Power drill	Preparation of the final report	Done
13, 14	Report writing and further testing	N/A	N/A	N/A	Done

Table A.2: Project Plan

## A.4 Design Drawings

### Main Parachute

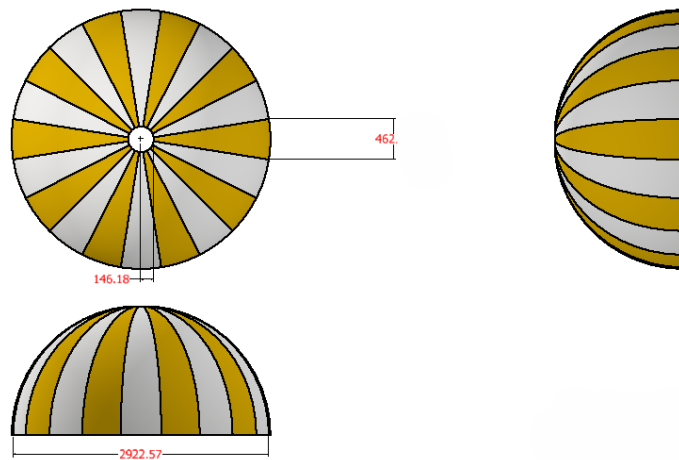


Figure A.2: main parachute

### Drogue Parachute

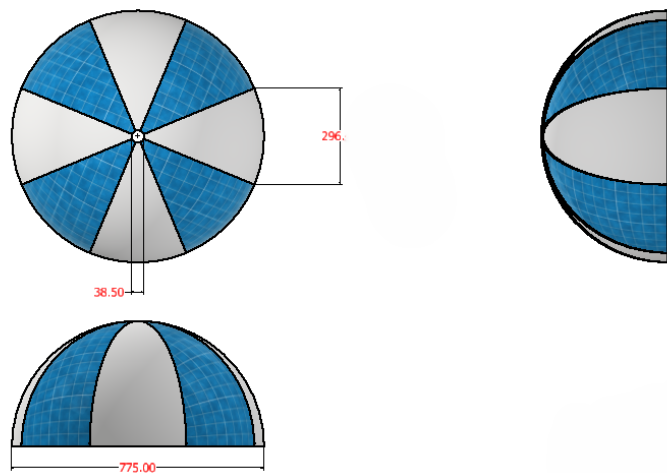


Figure A.3: drogue chute

### Avionics bay sub assembly

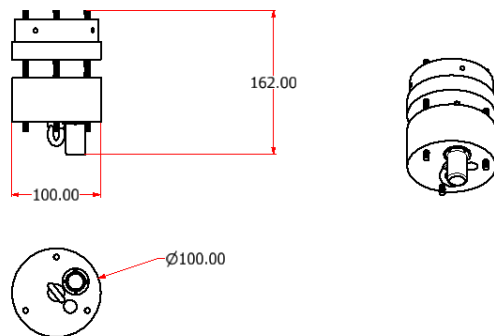


Figure A.4: avionics bay sub assembly

### Avionics bay lid

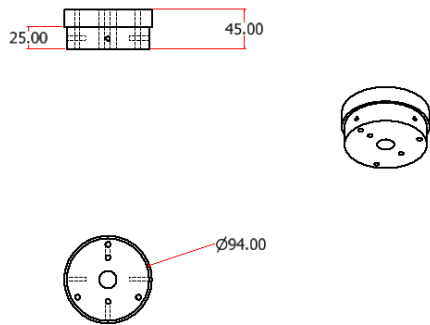


Figure A.5: avionics bay lid

### Avionics bay protector

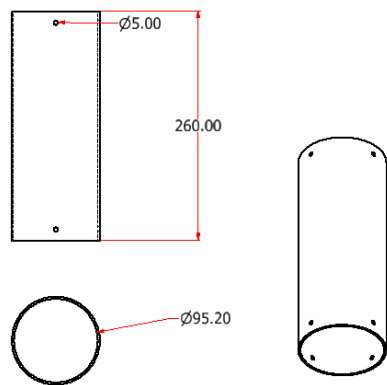


Figure A.6: avionics bay protector

### Bulkhead

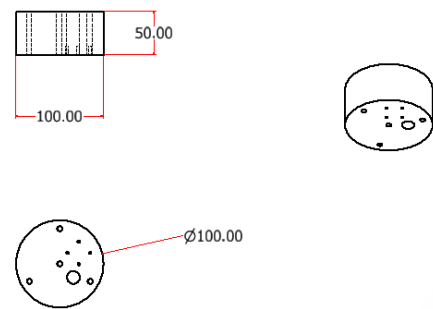


Figure A.7: bulkhead

### Charge protector

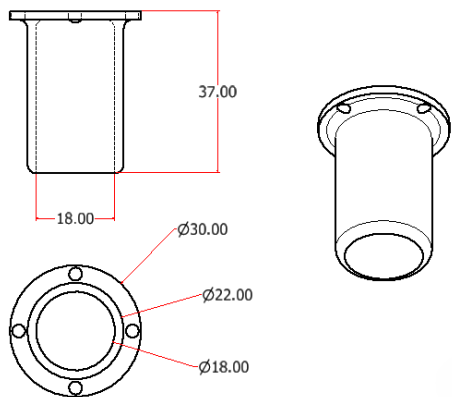


Figure A.8: charge holder

### Eye bolt

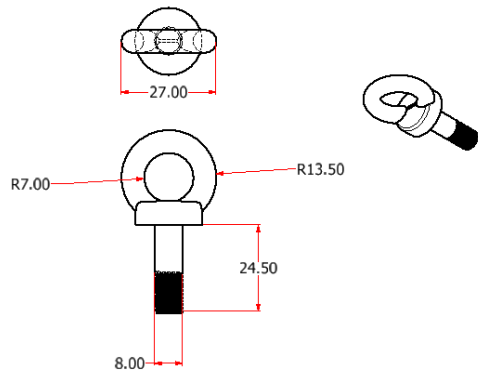


Figure A.9: eye bolt

### Shear pin

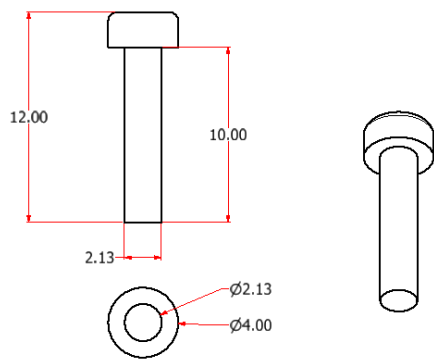


Figure A.10: shear pin

### Avionics Bay Assembly

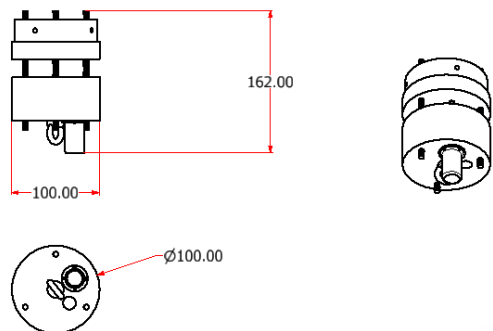


Figure A.11: Avionics Bay Assembly